Received 22 November 2013
Revised 3 March 2014
Accepted 22 May 2014

All-atom molecular-level computational simulations of planar longitudinal shockwave interactions with polyurea, soda-lime glass and polyurea/glass interfaces

Mica Grujicic, Ramin Yavari, Jennifer Snipes and S. Ramaswami
Department of Mechanical Engineering, Clemson University, Clemson, South Carolina, USA, and
Roshdy Barsoum
Ships and Engineering Systems Division, Office of Naval Research, Arlington, Virginia, USA

Abstract

Purpose – The purpose of this paper is to study the mechanical response of polyurea, soda-lime glass (glass, for short), polyurea/glass/polyurea and glass/polyurea/glass sandwich structures under dynamic-loading conditions involving propagation of planar longitudinal shockwaves.

Design/methodology/approach – The problem of shockwave generation, propagation and interaction with material boundaries is investigated using non-equilibrium molecular dynamics. The results obtained are used to construct basic shock Hugoniot relationships associated with the propagation of shockwaves through a homogeneous material (polyurea or glass, in the present case). The fidelity of these relations is established by comparing them with their experimental counterparts, and the observed differences are rationalized in terms of the microstructural changes experienced by the shockwave-swept material. The relationships are subsequently used to predict the outcome of the interactions of shockwaves with polyurea/glass or glass/polyurea material boundaries. Molecular-level simulations are next used to directly analyze the same shockwave/material-boundary interactions.

Findings – The molecular-level simulations suggested, and the subsequent detailed microstructural analyses confirmed, the formation of topologically altered interfacial regions, i.e. polyurea/glass and glass/polyurea interphases.

Originality/value – To the authors' knowledge, the present work is a first attempt to analyze, using molecular-level simulation methods, the interaction of shockwaves with material boundaries.

Keywords Polyurea, Material interface, Shockwaves, Soda-lime glass

Paper type Research paper

1. Introduction

In the present work, advanced non-equilibrium molecular-level computational methods and tools are used to investigate phenomena related to the generation, propagation and interaction of shockwaves within polyurea, soda-lime glass and polyurea/soda-lime-glass interfaces. Thus, the main aspects of the present work include: polyurea; soda-lime glass; molecular-level modeling of shock generation, propagation and interaction phenomena in polyurea; and molecular-level modeling of the same phenomena in

Multidiscipline Modeling in Materials and Structures
Vol. 10 No. 4, 2014
pp. 474-510

1573-6105
DOI 10.1108/MMMS-11-2013-0070

Report Documentation Page

Form Approved
OMB No. 0704-0188

1. REPORT DATE	2. REPORT TYPE	3. DATES COVERED
2014		**00-00-2014 to 00-00-2014**

4. TITLE AND SUBTITLE	5a. CONTRACT NUMBER
All-atom Molecular-level Computational Simulations of Planar Lngitudinal Shockwave Interactions with Polyurea, Soda-lime Glass and Polyurea/glass Interfaces	5b. GRANT NUMBER
	5c. PROGRAM ELEMENT NUMBER
6. AUTHOR(S)	5d. PROJECT NUMBER
	5e. TASK NUMBER
	5f. WORK UNIT NUMBER
7. PERFORMING ORGANIZATION NAME(S) AND ADDRESS(ES) **Clemson University,Department of Mechanical Engineering,241 Engineering Innovation Building,Clemson,SC,29634**	8. PERFORMING ORGANIZATION REPORT NUMBER
9. SPONSORING/MONITORING AGENCY NAME(S) AND ADDRESS(ES)	10. SPONSOR/MONITOR'S ACRONYM(S)
	11. SPONSOR/MONITOR'S REPORT NUMBER(S)

12. DISTRIBUTION/AVAILABILITY STATEMENT
Approved for public release; distribution unlimited

13. SUPPLEMENTARY NOTES

14. ABSTRACT

Purpose ??? The purpose of this paper is to study the mechanical response of polyurea, soda-lime glass (glass, for short), polyurea/glass/polyurea and glass/polyurea/glass sandwich structures under dynamic-loading conditions involving propagation of planar longitudinal shockwaves. Design/methodology/approach ??? The problem of shockwave generation, propagation and interaction with material boundaries is investigated using non-equilibrium molecular dynamics. The results obtained are used to construct basic shock Hugoniot relationships associated with the propagation of shockwaves through a homogeneous material (polyurea or glass, in the present case). The fidelity of these relations is established by comparing them with their experimental counterparts and the observed differences are rationalized in terms of the microstructural changes experienced by the shockwave-swept material. The relationships are subsequently used to predict the outcome of the interactions of shockwaves with polyurea/glass or glass/polyurea material boundaries. Molecular-level simulations are next used to directly analyze the same shockwave/material-boundary interactions. Findings ??? The molecular-level simulations suggested, and the subsequent detailed microstructural analyses confirmed, the formation of topologically altered interfacial regions, i.e. polyurea/glass and glass/polyurea interphases. Originality/value ??? To the authors??? knowledge, the present work is a first attempt to analyze using molecular-level simulation methods, the interaction of shockwaves with material boundaries.

15. SUBJECT TERMS

16. SECURITY CLASSIFICATION OF:			17. LIMITATION OF ABSTRACT	18. NUMBER OF PAGES	19a. NAME OF RESPONSIBLE PERSON
a. REPORT	b. ABSTRACT	c. THIS PAGE			
unclassified	**unclassified**	**unclassified**	**Same as Report (SAR)**	**37**	

soda-lime glass. A brief overview of these aspects of the problem at hand is presented in the remainder of this section.

1.1 Polyurea

Polyurea falls into a class of elastomeric co-polymers which are synthesized via a fast chemical reaction between difunctional isocyanate (OCN– R′–NCO) and difunctional amine (H_2N–R–NH_2) precursors. The first precursor contains isocyanate (–N = C = O) groups and an aromatic moiety (R′) while the latter contains amine (–NH_2) groups and a linear hydrocarbon chain (R). The resulting single-chain molecular structure consists of alternating hard segments (HS) and soft segments (SS). A typical chemical makeup of these segments is depicted schematically in Figure 1. Examination of Figure 1 reveals the presence of two "urea linkages" per HS. Due to high polarity of the urea linkages, and the presence of lone electron pairs on oxygen and nitrogen atoms (the conditions which are conducive to the formation of hydrogen bonds), and possible Π-type interactions which may promote ring stacking, HSs of the adjacent chains (or of the same chain) are subjected to strong attractive forces which promote their self-assembly/clustering. Consequently, bulk polyurea is typically not homogeneous but rather segregated, at a nano-meter-length-scale, into the discrete, rod-shaped, so-called "hard domains" which are dispersed throughout a continuous "soft matrix." Hard domains contain a high glass transition temperature, T_g, hydrogen-bonded phase which controls the overall stiffness and strength of polyurea (Grujicic *et al.*, 2010a, 2011a, c, d, 2012f). On the other hand, the soft matrix consists of a low-T_g compliant phase which is responsible for the high ductility of polyurea. Typical nano-meter-length-scale microstructure of polyurea as revealed using tapping-mode atomic force microscopy is shown in Figure 2 (Grujicic *et al.*, 2011d). The presence of rod-shaped hard domains is evident in this figure. Since inter-chain bonding in polyurea is mainly the result of the strong hydrogen bonding, polyurea is often referred to as being a thermo-plastically cross-linked polymer. However, depending on the fraction of isocyanate functional groups with functionality (defined as the number of mer's dangling bonds, which participate in the polymerization) > 2.0, polyurea may also be partly cross-linked. It is established (e.g. Castagna *et al.*, 2012) that polyurea properties are greatly affected by the relative contributions of hydrogen-bonding and covalent-bonding-based cross-linking.

While polyurea has been traditionally known as a material with superior wear resistance, recent experimental and computational studies (e.g. Bogoslovov *et al.*, 2007; Grujicic *et al.*, 2010c, 2011b, 2012h) have demonstrated that this material also possesses an unusually high potential for: first, increasing the ballistic penetration performance of metallic and construction-material structures; and second, dispersion/attenuation of the shockwaves resulting from blast and/or ballistic impact loading. Recently, the potential use of polyurea as advanced combat helmet coating/lining and/or suspension-pad material has been explored (Grujicic *et al.*, 2010a, 2011b, 2012e, f, h, j). When used in these applications, the main role of polyurea is to mitigate blast effects and reduce undesirable consequences related to mild traumatic brain injury.

1.2 Soda-lime glass

One of the basic properties of all types of glass is their lack of long-range atomic order which classifies them as amorphous materials. For instance, the atomic arrangement in pure silicate glass (i.e. fused silica) is highly random relative to the chemically equivalent (crystalline) quartz. To describe the random atomic arrangement within glass the so-called "random network model" (Kingery *et al.*, 1976) is typically employed. Such a

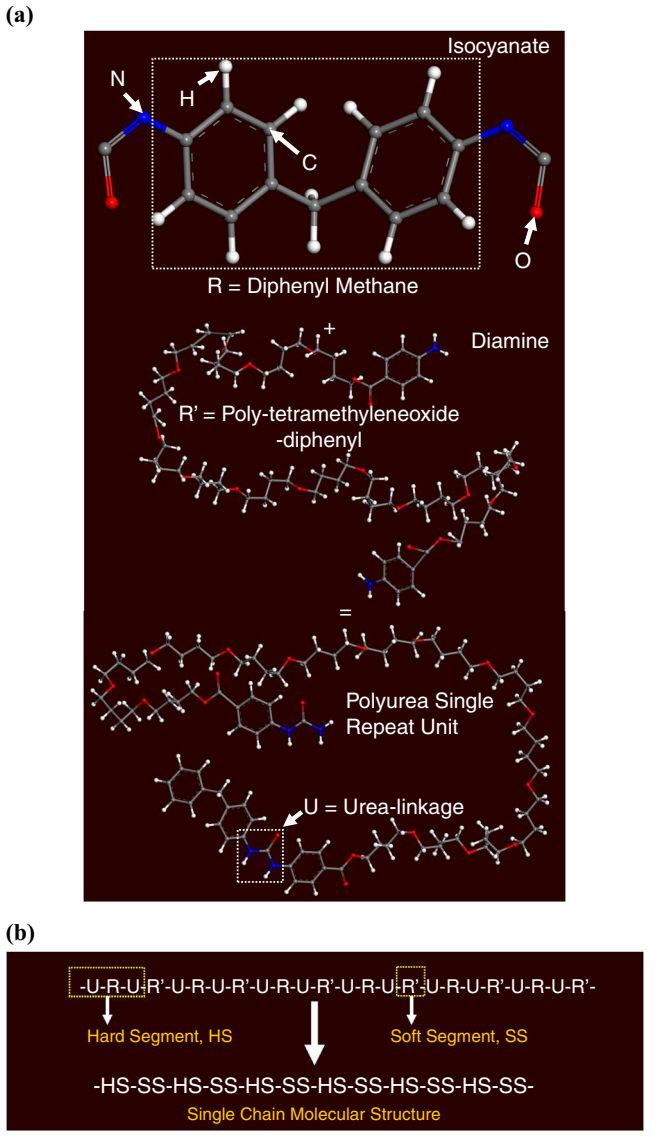

Figure 1.
(a) Co-polymerization reaction resulting in the formation of segmented polyurea; and (b) Simplified notation for polyurea structure using functional groups U (Urea linkage), R (Diphenyl Methane) and R' (Poly-tetramethyleneoxide-diphenyl) and the corresponding definitions of hard segments and soft segments

model represents amorphous materials as a three-dimensional linked network of polyhedra with central cations of various coordination depending on the character of the atomic constituents. In the case of silicate-based glasses like fused silica and soda-lime glass, the dominant cation is silicon. In this case, each silicon is surrounded by four oxygen anions and forms a SiO_4^{4-} tetrahedron, whereby each oxygen is bonded to (or bridges) two silicon atoms. Other polyhedra may exist in the network depending on the glass additives. Since silicon has a tendency to form a continuous network with (bridging) oxygen atoms, SiO_2 is commonly referred to as a "network former." Other potential network formers in glass are boron and germanium oxides.

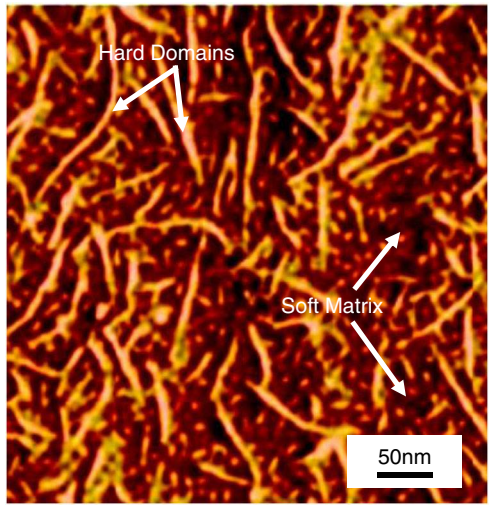

Figure 2.
An example of a typical tapping-mode atomic force microscopy (AFM) image of a polyurea showing a rod-like morphology of the hard segments

Numerous oxides and other additives are used to modify the basic silica tetrahedra network of silicate-based glasses in order to tailor their properties to specific applications. When alkali (or alkaline earth) oxides are added to a pure silicate-based glass, in order to accommodate the excess of oxygen anions which are present due to the oxide dissociation, the continuity of the silica tetrahedra network becomes disrupted. The resulting glass structure contains additional non-bridging (connected to only one silicon atom) oxygen atoms. Charge transfer from the alkaline earth metal atoms converts the non-bridging oxygen atoms into singly charged anions. The metallic cations formed in this process tend to hover around the non-bridging oxygen ions for local charge neutrality. Since alkali (or alkaline earth) based oxides cause a disruption in the continuous glass network, they are typically referred to as "network modifiers." In the case of soda-lime glass (material analyzed in the present work), the 14 wt.% Na_2O and 9 wt.% CaO additions to the silica both act as network modifiers. An example of the local atomic structure in soda-lime glass is shown in Figure 3.

In contrast to network-modifying oxides, more covalently bonded oxides like B_2O_3 donate metallic cations which become incorporated into the glass network without a

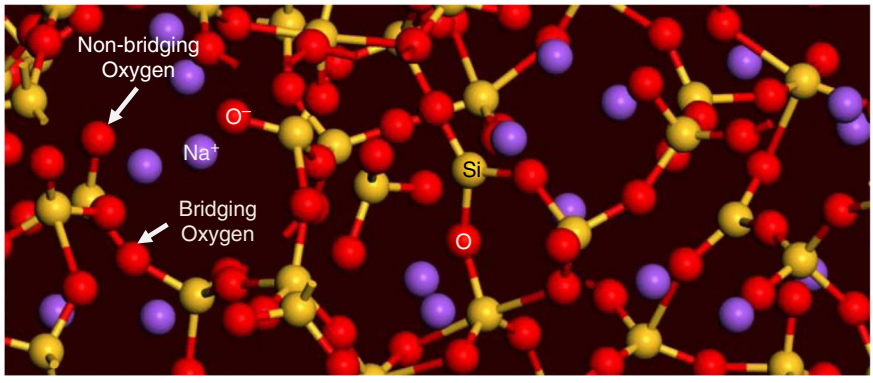

Figure 3.
An example of the local atomic structure in soda-lime glass

significant compromise in the network connectivity. In other words, the addition of these oxides does not lead to the formation of non-bridging oxygen atoms. Due to the aforementioned behavior of these glass-oxide additives, they are typically referred to as network formers.

For the purpose of quantitative description of the microstructure within the random network model, a number of network parameters have been introduced. For instance, a so-called *R*-value (defined as the average number of oxygen ions per network-forming ion) is used to describe the overall connectivity of a given network. In the case of fused silica, in which there are two (bridging) oxygen anions for every network-forming silicon cation, the *R*-value is 2.0. In the case of soda-lime glass, the introduction of non-bridging oxygen ions causes the *R*-value to increase to ca. 2.41. This finding suggests that a higher *R*-value is associated with a more open (less connected) weaker amorphous glass network. As far as the network formers are concerned, their effects on the glass microstructure and the *R*-value is greatly affected by the cation coordination number and the strength of its bond with oxygen as well as to the concentration of the additive. In addition to the *R*-value, the so-called "*X*" and "*Y*" parameters are often used to further quantify the glass network structure. These two parameters are, respectively defined as the average number of non-bridging (connected to only a single network-forming cation) and bridging (connected to two network-forming cations) oxygen atoms per network polyhedron. Since pure silicate-based glasses contain only bridging oxygen atoms (and are based on silica tetrahedra), the *X* and *Y* parameters take on values of 0.0 and 4.0, respectively. On the other hand, since soda-lime glass contains additional non-bridging oxygen atoms (while its network is still based on silica tetrahedra), *X* takes on a non-zero value (ca. 0.81) while *Y* drops below 4.0 (ca. 3.19).

In addition to chemical modifications of glass, changes in the microstructure of this material can be brought about by mechanical loading/deformation (typically requiring several GPa pressure levels). Specifically, high pressure may result in a reorganization of the atomic network (phase change) in the form of changes to the coordination of the network-forming cations. These phase changes can be of first order, which are characterized by the formation of a distinct high-pressure phase at a nominally constant pressure, or they may be of second order, which are phase changes which involve a continuous morphing of the original phase into the final high-pressure phase over a range of pressures. These phase transformations may be associated with significant volume changes and, since phase-transformation-induced energy absorption is a well-documented phenomenon responsible for high toughness levels in TRIP steels and partially stabilized crystalline ceramics, it is of interest to the present study.

There are first-order phase transformations in soda-lime glass which occur in the pressure-range of 3-5 GPa, and are associated with relatively modest (3-7 percent) volume changes (Grujicic *et al.*, 2011g, h, 2012d, g). These phase-transformations should not be confused with those seen to take place at substantially higher pressures (ca. >20 GPa), which are considered to be of second order and associated with substantially larger volume reductions and with the formation of stishovite, an octahedrally coordinated glass phase.

1.3 Molecular-level computational analyses of shockwaves in Polyurea

Examination of the recent open literature revealed that molecular-level analyses of shockwave phenomena in polyurea have been conducted using both all-atom and

coarse-grained non-equilibrium methods and tools. Grujicic *et al.* (2011f) utilized the so-called unit-cell uniaxial-contraction method to generate a pair of converging shocks in an all-atom nano-segregated polyurea model. The results obtained are used to: generate the basic shock-Hugoniot relations in polyurea; identify different (inelastic-deformation and energy-dissipation) phenomena/processes taking place at, or in the vicinity of, the shock front; and help elucidate the molecular-level character of these phenomena/processes.

The approach developed by Grujicic *et al.* (2011f) has been extended (Grujicic *et al.*, 2012i) to quantify contributions of the various shock-induced phenomena and processes to the ability of polyurea to mitigate shocks of various strengths. Regarding the coarse-grained molecular-level analysis of shockwave phenomena in polyurea, Grujicic *et al.* (2013b) utilized the unit-cell uniaxial-contraction method in order to address some of the potential shortcomings of all-atom computational methods (e.g. the shortcomings arising from the limited size of the computational domain, inadequate level of nano-scale segregation, limitation to modeling strong shockwaves with small wavefront-width, etc.). Within the coarse-grained computational methods, hypothetical particles called beads are used to represent an ensemble of neighboring atoms and to account for their collective dynamic behavior. Due to the larger size of the beads, larger computational domains can be analyzed. Furthermore, since high-frequency vibration of the individual atoms is integrated out, longer computational step times and, thus, total times can be afforded. The results obtained suggested that the chemistry- (or, more specifically, the SS molecular weight) dependent extent of nano-scale phase segregation and of the degree of short-range order within the hard domains play an important role in the shock-mitigation ability of polyurea. In a subsequent coarse-grained molecular-level analysis of shockwave phenomena in polyurea, Grujicic *et al.* (2014b) demonstrated that shock-induced hard-domain densification makes an important contribution to the superior shock-mitigation capacity of polyurea, and that the extent of densification is a sensitive function of the polyurea SS molecular weight. In particular, the ability of release-waves to capture and neutralize shockwaves (an important mitigation process in the case of blastwave-induced shockwaves) was found to depend strongly on the (polyurea-chemistry and synthesis-route dependent) extent of shock-induced hard-domain densification.

1.4 Molecular-level computational analyses of shockwaves in soda-lime glass

Grujicic *et al.* (2011h) employed all-atom molecular-level modeling and simulations to study room-temperature micro-structural and mechanical response of soda-lime glass when subjected to high (i.e. several GPa) uniaxial-strain stresses/pressures. The results obtained revealed the occurrence of an irreversible phase-transformation (accompanied by a permanent 3-7 percent volume reduction) starting at a stress/pressure of ca. 4 GPa. Close examination of molecular-level topology revealed that the pressure-induced phase transformation in question is associated with an increase in the average coordination number of the silicon atoms, and the creation of two to fourfold (smaller, high packing-density) Si-O rings. The associated loading and unloading axial-stress vs specific-volume isotherms were next converted into the corresponding loading Hugoniot and unloading isentrope axial-stress vs specific-volume relations. These were subsequently used to analyze the role of the pressure-induced phase-transformation/irreversible-densification in mitigating the effects of blast- and ballistic-impact loading onto a prototypical glass plate used in monolithic and laminated transparent armor applications. The results of this part of the work revealed that pressure-induced

phase-transformations can provide several beneficial effects such as lowering of the loading/unloading stress-rates and stresses, increased shockwave dispersion, and increased energy absorption.

In a subsequent work, Grujicic *et al.* (2012d) employed the aforementioned unit-cell uniaxial-contraction method within the all-atom environment in order to directly generate and characterize shockwaves within soda-lime glass. The results obtained confirmed that the aforementioned processes indeed play a critical role in the ability of soda-lime glass to attenuate and disperse shockwaves. The analysis further yielded the basic shock Hugoniot relations for soda-lime glass. The availability of a shock Hugoniot is critical for construction of a high deformation-rate, large-strain, high-pressure material model which can be used within a continuum-level computational analysis to capture the response of a soda-lime glass based laminated transparent armor structure (e.g. a military vehicle windshield, door window, etc.) to blast-/ballistic-impact loading.

1.5 Main objectives

The main objectives of the present work can be summarized as follows:

(1) To carry out an all-atom molecular-level non-equilibrium computational investigation of shock generation and propagation in polyurea and soda-lime glass, as well as of the interaction of these waves with the polyurea/glass and glass/polyurea material boundaries.

(2) To compare the results obtained with their continuum-level counterparts as yielded by the conventional planar longitudinal shockwave analysis.

(3) To analyze changes experienced by the material through which the incident shock passes, as well as changes in the interfacial region resulting from the interaction of the incident shock with the material boundary in question. These changes in the material microstructure are to be used in order to help clarify the observed differences between the molecular-level simulation results and their continuum-level counterparts.

1.6 Paper organization

A brief overview of the molecular-level computational procedure including the computational cell construction, forcefield identification, computational method(s) selection, shock-wave generation and the problem definition are, respectively presented in Sections 2.1-2.5. The key results obtained in the present work are presented and discussed in Section 3. A summary of the key findings and concluding remarks are given in Section 4.

2. Molecular-level computational analyses

In the present work, formation and propagation of planar longitudinal shocks within polyurea, glass, polyurea/glass/polyurea and glass/polyurea/glass sandwich structures is investigated using molecular-level computational methods and tools. These methods and tools consider a material as a system of interacting (and bonded) discrete particles (i.e. atoms, ions, etc.) and utilize potential-energy-minimization based (molecular statics) and Newton's second law based (molecular dynamics) algorithms to examine and quantify the behavior and properties of the material under investigation. It is generally recognized that molecular-level computational methods and tools provide a good compromise between: ab-initio quantum mechanics methods, the methods which are intrinsically more accurate but limited to material systems containing no more than a

few hundred interacting particles; and meso-scale (also known as coarse-grained) computational methods, the methods which enable analysis of larger computational domains but rely on the concept of beads, larger hypothetical particles.

In general, complete definition of a molecular-level computational model and analysis requires specification of: geometrical (e.g. atomic positions, computational-cell size, etc.) and chemical (e.g. atomic species, bond order, etc.) details of the computational model; a set of fully-parameterized force-field functions (inter-atomic potentials); and details regarding the type, the number and the usage sequence of the molecular-level computational algorithms/methods to be used in the simulation. In addition to these three aspects of the computational model/analysis, a procedure had to be introduced, in the present work, for generation of planar longitudinal shockwaves within the material molecular systems. More details of these four aspects of the present computational effort, as well as of the problem analyzed in the present work, are presented in the remainder of this section.

2.1 Molecular-level computational model

2.1.1 Polyurea. To construct the computational model for polyurea, the procedure developed in our prior work (Grujicic *et al.*, 2011f, 2012i) was followed. Within this procedure, a rectangular parallelepiped-shaped computational unit-cell (extended in the direction of the propagating planar shockwaves) is constructed. To prevent spurious effects associated with the presence of free-surfaces, periodic boundary conditions are imposed across the cell faces. The three edges ($a = b < c$) of the cell are aligned, respectively with the three global coordinate axes (x, y and z). The procedure developed by Grujicic *et al.* (2011f, 2012i) involves the following steps: first, construction of a single repeat unit; second, construction of a single chain; third, construction of multiple chains and their placement into the computational cell; and fourth, rearrangement of the chains to obtain the necessary level of material segregation in the initial state of polyurea. Steps (a)-(b) were done using the Visualizer program from Accelrys (I), step (c) was completed using the Amorphous Cell program, also from Accelrys (II), while step (d) was executed using an in-house developed computer program. Since these details of the molecular-level computational-model construction can be found in Grujicic *et al.* (2011f, 2012i), they will not be repeated here. Figure 4(a) shows a prototypical computational cell for polyurea used in the present work.

2.1.2 Soda-lime glass. As in the case of polyurea, the computational model for soda-lime glass involves a rectangular parallelepiped-shaped computational cell, extended in the direction of shockwave propagation and subjected to the periodic boundary condition across its faces. The three edges ($a = b < c$) of the cell are again aligned, respectively with the three global coordinate axes. To construct the computational cell for soda-lime glass, the procedure developed in our prior work (Grujicic *et al.*, 2011h, 2012d) was followed. This procedure involves the following steps:

(1) construction of a short silica-chain fragment, using the Visualizer program (I);

(2) growth of the fragment generated in (a) by a duplicate-and-attach process using the same program, to construct a glass network structure. Simultaneously, sodium cations are added to counterbalance the non-bridging oxygen ions; and

(3) packing of the glass network and sodium ions into the computational cell using the Amorphous Cell program (II), while ensuring that the target mass density of 2.613 g/cm^3 is reached.

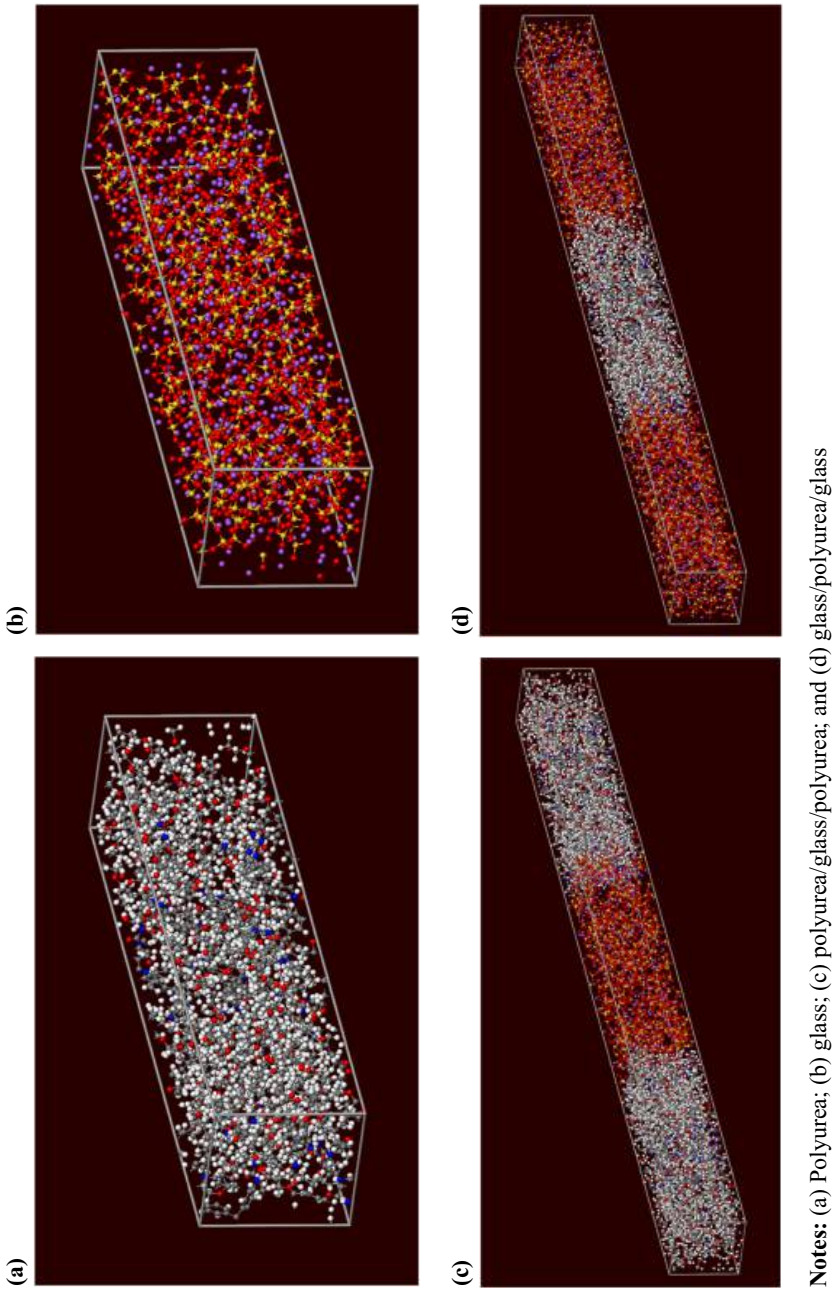

Notes: (a) Polyurea; (b) glass; (c) polyurea/glass/polyurea; and (d) glass/polyurea/glass

Figure 4.
Computational cells

Figure 4(b) shows a prototypical computational cell for soda-lime glass used in the present work.

2.1.3 Polyurea/glass/polyurea. To construct the computational model for the polyurea/glass/polyurea sandwich structure, two polyurea computational unit-cells (described above) are used to sandwich a single soda-lime glass unit-cell (also described above) in the z-direction (the direction of shockwave propagation). This procedure required that the polyurea and the soda-lime glass unit-cells have identical edge lengths in the x- and in the y-directions. Figure 4(c) shows a prototypical computational cell for polyurea/glass/polyurea sandwich structure used in the present work.

2.1.4 Glass/polyurea/glass. To construct the computational model for the glass/polyurea/glass sandwich structure, two glass computational unit-cells are used to sandwich a single polyurea unit-cell in the z-direction. Again, this procedure required that the soda-lime-glass and the polyurea unit-cells have identical edge lengths in the x- and in the y-directions. Figure 4(d) shows a prototypical computational cell for glass/polyurea/glass sandwich structure used in the present work.

2.2 Force-fields

It is well recognized that the overall utility of molecular-level computational analyses is highly affected by fidelity and accuracy of the employed force-field (a set of mathematical expressions which quantify the contribution of various bonding and non-bonding interactions between the constituents of the molecular-scale model to the material system potential energy). The present work utilizes the so-called "Condensed-phase Optimized Molecular Potentials for Atomistic Simulation Studies" (COMPASS) force-field (Sun, 1998; Sun *et al.*, 1998). This highly accurate force-field is of an ab-initio character since most of its parameters were established by matching the predictions made by the ab-initio quantum mechanics calculations with their experimental counterparts.

Within the COMPASS force-field, the potential energy of a system of bonded and interacting particles is expressed as a sum of: the valence (or bond), $E_{valence}$; the cross-term, $E_{cross\text{-}term}$; and the non-bond, $E_{non\text{-}bond}$, interaction energies as:

$$E_{total} = E_{valence} + E_{cross-term} + E_{non-bond} \tag{1}$$

The valence energy, in turn, contains the following components: a bond stretching term, E_{bond}; a two-bond included-angle term, E_{angle}; a three-bond-dihedral-torsion term, $E_{torsion}$; an inversion (or an out-of-plane interaction) term, E_{oop}; and a Urey-Bradlay term (involves interactions between two atoms bonded to a common atom), E_{UB}, as:

$$E_{valence} = E_{bond} + E_{angle} + E_{torsion} + E_{oop} + E_{UB} \tag{2}$$

The cross-term interacting energy, $E_{cross\text{-}term}$, accounts for the interaction of various valence components of the potential energy and includes interaction energies involving: stretch-stretch interactions between two adjacent bonds, $E_{bond\text{-}bond}$; stretch-bend interactions between a two-bond angle and one of its bonds, $E_{bond\text{-}angle}$; bend-bend interactions between two valence angles associated with a common vertex atom, $E_{angle\text{-}angle}$; stretch-torsion interactions between a dihedral angle and one of its end bonds, $E_{end\_bond\text{-}torsion}$; stretch-torsion interactions between a dihedral angle and its middle bond, $E_{middle\_bond\text{-}torsion}$; bend-torsion interactions between a dihedral angle and

one of its valence angles, $E_{angle\text{-}torsion}$; and bend-bend-torsion interactions between a dihedral angle and its two valence angles, $E_{angle\text{-}angle\text{-}torsion}$, terms as:

$$E_{cross-term} = E_{bond-bond} + E_{angle-angle} + E_{bond-angle} + E_{end\_bond-torsion} + E_{middle\_bond-torsion} + E_{angle-torsion} + E_{angle-angle-torsion} \quad (3)$$

The non-bond interaction term, $E_{non\text{-}bond}$, accounts for the interactions between non-bonded atoms and includes: the van der Waals energy, E_{vdW}; and the Coulomb electrostatic energy, $E_{Coulomb}$, as:

$$E_{non-bond} = E_{vdW} + E_{Coulomb} \quad (4)$$

Analytical expressions for various bond and non-bond interaction energies appearing in Equations (1)-(4) as used by the COMPASS force-field functions can be found in our previous work (Grujicic and Lai, 1999).

2.3 Computational methods

Two types of computational methods are employed in the present work:

(1) molecular statics; and

(2) molecular dynamics.

These methods are implemented in Discover, a molecular-level simulation program from Accelrys (III).

2.3.1 Molecular statics. The molecular statics method is essentially a constrained-optimization technique within which the potential energy (objective function) of the computational cell (as defined by Equations (1)-(4)) is minimized with respect to the position of the constituent atoms/ions (design variables) subjected to constraints related to the imposed periodic boundary conditions. The potential energy minimization within Discover (III) is conducted by adaptively engaging and disengaging the Steepest Descent, Conjugate Gradient and the Newton's minimization algorithms. That is, the Steepest Descent method is employed in the earliest stages of the minimization procedure in order to efficiently arrive at a molecular-level configuration which is quite close to its optimum counterpart (i.e. the one associated with the minimum potential energy). On the other hand, in the latest stages of the minimization procedure, the Newton's algorithm is employed which ensures a monotonic and stable transition of the material into its optimal configuration.

Molecular statics is employed to minimize the potential energy of the newly constructed computational cells (described in Section 2.1). In addition, as will be discussed in greater detail in Section 3, this method is also employed to help quantify the state of the material swept by a shockwave.

2.3.2 Molecular dynamics. Within the molecular dynamics method, negative gradient of the potential energy evaluated at the location of each atom is first used to compute forces acting on each atom. Then, the associated Newton's equations of motion (three equations for each atom) are integrated numerically with respect to time in order to determine the temporal evolution of the material molecular-level configuration. Molecular dynamics methods are generally classified into the equilibrium and non-equilibrium methods, and both of these methods are employed in the present work.

Within the equilibrium molecular-dynamics methods, the subject material system is maintained in the state of thermal-mechanical equilibrium by coupling it to the surroundings, such as a constant pressure bath, a constant temperature reservoir, etc. This ensures the absence of net flux of the mass, momentum and energy in any of the three principal coordinate directions. In the present work, NVT (where N is the (fixed) number of atoms, V, the computational-cell volume (also fixed), and T ($= 298$ K) is the temperature) equilibrium molecular dynamics is employed in the first stage of the shock generation procedure (more details of this procedure will be provided in the next section).

Within non-equilibrium molecular dynamics, the system is subjected to large mechanical and/or thermal perturbations (finite changes in the axial parameter of the computational cell, in the present case). As a consequence, the system experiences large fluxes of its thermodynamic quantities (mass, momentum and energy, in the present case). Since Discover was initially designed to carry out equilibrium molecular-dynamics simulations, a procedure had to be devised to deactivate "equilibration" portions of this algorithm so that non-equilibrium molecular-dynamics calculations can be carried out.

2.4 Generation of molecular-level shockwaves

Since the materials analyzed in the present work are of a bulk type (which was accomplished through the use of periodic boundary conditions), molecular-level shockwaves could be generated only in pairs (i.e. two shocks per unit cell). The procedure employed in the present work to generate molecular-level shocks, relies on a step-wise sequential contraction of the computational-cell longitudinal lattice parameter, c. Due to the use of the periodic boundary conditions in the longitudinal direction, this shockwave-generation procedure is analogous to the so-called "symmetric flyer-plate test" (Amirkhizi *et al.*, 2006), within which a flyer-plate impacts normally (i.e. at a zero-obliquity angle) a target plate (where the two plates are made of the same material). Within the symmetric flyer-plate test, two identical diverging shockwaves are generated, one within the flyer-plate and the other within the target plate. Exactly the same scenario is encountered in the present shockwave-generation procedure. However, due to the use of the periodic boundary conditions in the longitudinal direction, this procedure initially yields a pair of identical converging shockwaves within the computational cell.

To generate a pair of converging shockwaves within the unit cell, the following procedure is employed: first, before the shockwaves are introduced, a "sufficiently long" NVT molecular dynamics simulation is conducted in order to thermally equilibrate the system at its target temperature (298 K); second, the thermal-equilibration algorithm is disabled in order to allow Discover to run in a non-equilibrium molecular-dynamics mode; third, the shocks are then initiated (and driven) by continuously contracting the computational-cell longitudinal lattice-parameter c as:

$$c(t) = c(t = 0) - 2u_p t \tag{5}$$

where t denotes time and u_p is the desired/pre-selected particle velocity (of the material swept by either of the shockwaves) in the z-direction. In the present work, u_p is varied in a 200-1,000 m/s range in order to simulate the generation and propagation of shockwaves of various strengths; and fourth, during the application of the shock-generation procedure, computational-cell transverse lattice parameters a and b are kept constant in order to obtain planar, longitudinal (i.e. uniaxial-strain) shock conditions.

The molecular-level shockwave-generation procedure described above results in the formation of two converging identical shockwaves (at the computational-cell longitudinal faces), each moving toward the computational-cell center at a shock speed U_s. The passage of these shocks through the material causes an abrupt and substantial increase in the material mass density, internal-energy density, stress, particle velocity, temperature and entropy density. Furthermore, interactions of these shockwaves with the polyurea/glass and glass/polyurea material interfaces results in the formation of transmitted shockwaves and reflected shock-/release-waves.

The aforementioned procedure for molecular-level shock-wave generation, including the initial thermal-equilibration molecular-dynamics based procedure, is conducted through the use of a Discover input file (III). This file is written using the Basic Tool Command Language which enabled the use of a scripting engine that provides very precise control of simulation tasks, e.g. sequential contraction of the computational cell in the longitudinal direction, deactivation of the thermal-equilibration algorithm during the shock-generation process, etc.

2.5 Problem formulation

The problem addressed in the present work can be summarized as follows: (a) the computational procedures described in the previous sections are used to construct molecular-level computational cells and the resident converging shocks of various strengths; (b) the material-configuration/dynamics results are then used in a post-processing computational analysis in order to determine the basic shock-Hugoniot relations in polyurea and soda-lime glass; (c) a post-processing data-reduction procedure is developed to analyze interactions of the incident shockwaves with the polyurea/glass zand glass/polyurea material interfaces; and (d) the same materials as those used in (b) and (c) are next employed to identify the nature of the deformation and microstructure-altering processes at the shock front and in the vicinity of the material interfaces upon their interactions with the incident shock. These processes control the extent of dissipation of the energy carried by the incident, transmitted and reflected shockwaves.

3. Results and discussion

In this section, the main results pertaining to the molecular-level analysis of shockwave physics in polyurea, soda-lime glass, polyurea/glass/polyurea and glass/polyurea/glass sandwich structures are presented and discussed.

3.1 Polyurea

In this subsection, the basic procedures and results related to: the generation and propagation of incident shockwaves in polyurea; construction of the corresponding shock Hugoniot relations; and identification of the major shockwave-induced microstructural changes are presented and discussed.

3.1.1 Incident shockwave generation and propagation. An example of the typical results, obtained in this portion of the work, pertaining to the temporal evolution of polyurea molecular-level microstructure during the process of step-wise sequential contraction of the computational-cell longitudinal lattice parameter is shown in Figure 5(a)-(d). It should be noted that, for improved clarity, covalent bonds are not displayed in this figure and all the atoms are represented with the same color. The results displayed in Figure 5(a)-(d) clearly demonstrate the generation (at the computational-cell axial end faces) and propagation of a pair of converging planar, longitudinal shockwaves. An approximate location of the center-point of the two

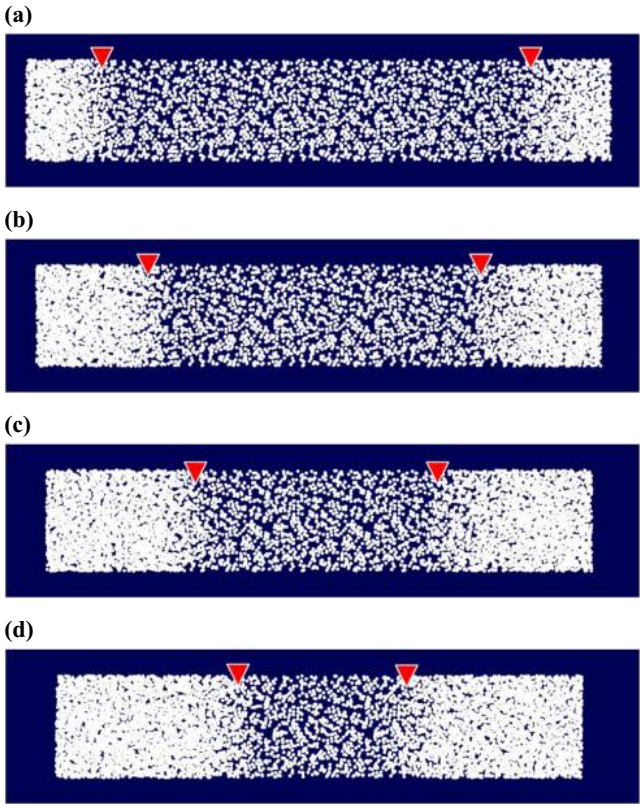

Figure 5.
Temporal evolution of the molecular-level material microstructure accompanying generation and propagation of a pair of converging planar shocks in polyurea

shocks is indicated using arrowheads in Figure 5(a)-(d). Typically the simulations are terminated before collision of the two shocks takes place, since phenomena related to shockwave/shockwave interactions is beyond the scope of the present work. The results displayed in Figure 5(a)-(d) show that the shockwaves remain fairly planar during their motion and that the "shocked" material (i.e. the material swept by the shocks) acquires a significantly higher mass/number density.

Now that the two converging shocks have been identified, the next task is to reveal the structure of their front. This is done using the following procedure. First, the original computational cell is partitioned (in the longitudinal direction, z) into (typically) 40 equal-size Lagrangian bins (the term "Lagrangian" is used here in order to denote that the bins are defined in the material reference/initial configuration) (Grujicic *et al.*, 2011e, 2014a, 2012b; Grujicic and Pandurangan 2012). Then, all the atoms associated with each bin are identified. It should be noted that, due to the Lagrangian nature of the bins used, the same atoms remain associated with a given Lagrangian bin throughout the process of shockwave generation and propagation. Lastly, average material/atomic properties for each cell (e.g. material-particle velocities, particle number-density, etc.) are computed at each simulation time.

Examples of the typical results obtained (for the right-propagating shockwave only) through the use of the procedure described above are displayed in Figure 6(a)-(b). The results displayed in Figure 6(a)-(b) are obtained under identical conditions

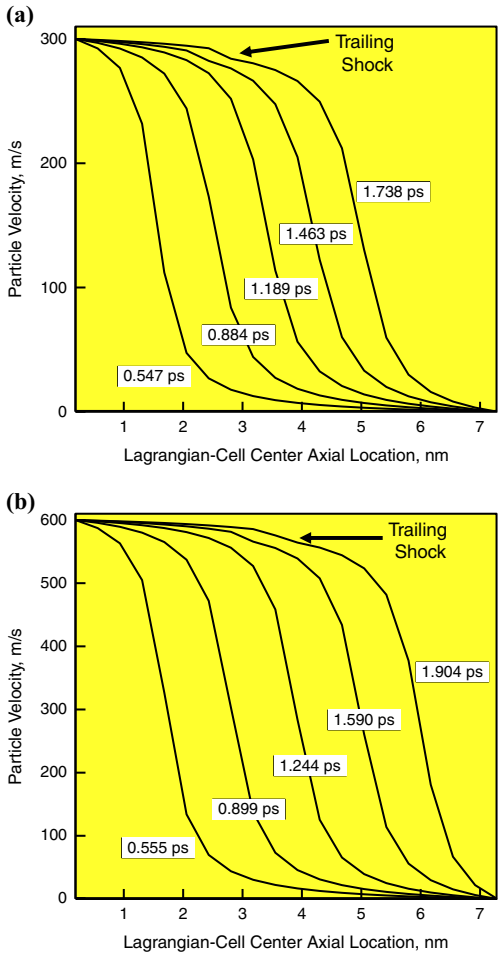

Figure 6.
Temporal evolution of the particle velocity associated with a right-propagating planar shockwave in polyurea under imposed (maximum) particle velocities

Notes: Curve labels pertain to the respective post-shock initiation times. (a) 300 m/s; (b) 600 m/s

except for the magnitude of the imposed shocked-material particle longitudinal velocity (300 m/s in the case of Figure 6(a) and 600 m/s in the case of Figure 6(b)). In these figures, particle (longitudinal) velocities at different simulation (i.e. post-shockwave-initiation) times are plotted against the Lagrangian bin center z-location. The simulation times expressed in ps are used to label the corresponding curves in Figure 6(a)-(b).

Examination of the results displayed in Figure 6(a)-(b) reveals that:

(1) After a brief transient period, the shockwaves appear to reach a steady wave profile (i.e. a wave-front form which is time-invariant relative to a moving frame which is attached to the shockwave front). It should be noted that, since no thermostat was used during the molecular-level shock-wave generation/propagation analysis, the attainment of the steady-wave condition is a natural

consequence of a balance between the continuous supply of linear longitudinal momentum to the system (through the step-wise sequential computational-cell longitudinal contraction) and the molecular-level deformation and microstructure-altering processes taking place at the shock front;

(2) As the shock strength increases, as measured by the imposed particle velocity, the shock speed increases while the shockwave-front thickness decreases. This behavior is identical to the one predicted by the continuum-level theory of shockwaves in solids (e.g. Davison, 2008);

(3) The results for the left-propagating shockwave (not shown for brevity) are quite similar, but not identical, to the ones displayed in Figure 6(a)-(b). This finding is expected considering the heterogeneous nature of the nano-segregated polyurea; and

(4) Also due to the heterogeneous nature of polyurea, shockwave-front profiles displayed in Figure 6(a)-(b) show some irregularities, and there is indication of the formation of trailing shockwaves. However, these shockwaves tend to vary in strength and speed as the main shockwave advances.

3.1.2 Determination of shock Hugoniot relations. The results presented in Figure 6(a)-(b) (and the corresponding results obtained at additional imposed particle longitudinal velocities) reveal the formation and propagation of steady shockwaves. These results can be used to determine a functional relationship between the (Lagrangian) shockwave speed, U_s (set equal to a ratio of the steady shockwave-front advancement and the associated elapsed time) and the particle velocity, u_p.

The results of the shockwave-speed computational procedure are displayed (the curve labeled "All-Atom") in Figure 7(a). For comparison, experimental results obtained in the work of Mock *et al.* (2009) (the curve labeled "Experimental") are also displayed in this figure.

The U_s vs u_p function is one of the so-called shock Hugoniot relations. The shock Hugoniot can be defined as a hyperline within a combined material-state/kinematic hyperspace which represents the locus of all possible shocked-material states, particle velocities and shockwave speeds, which can be attained (depending on the shockwave-strength) from a given material initial/reference state. The U_s vs u_p relation mentioned above could be interpreted as a simple projection of the Hugoniot hyperline to the U_s-u_p plane. In addition to the U_s vs u_p shock Hugoniot relation, other Hugoniot relations such as: (negative) longitudinal stress, $-t_{11}$, vs u_p; $-t_{11}$ vs normalized specific volume, v/v_0 (v_0 denotes the material initial specific volume); and (mass-based) internal energy density, e vs v/v_0, etc. are often used within the analysis of planar longitudinal shockwaves. It should be noted that, since all these relations are different planar projections of the same Hugoniot hyperline, they are all mutually related. Thus, the knowledge of one of these relations (U_s vs u_p, in the present case) enables determination of the remaining Hugoniot relations. In the present work, the procedure based on the use of the so-called "shock-jump equations" (a set of, for the case of a planar longitudinal shockwave, three non-linear algebraic equations) (Davison, 2008) which quantify the (abrupt and significant) changes in the material state and kinematic variables across the shockwave-front, was utilized to generate the additional three Hugoniot relations (mentioned above). The results of this procedure are shown in Figure 7(b)-(d). The corresponding experimental results obtained in the work of Mock *et al.* (2009) are also shown in these figures. It should be

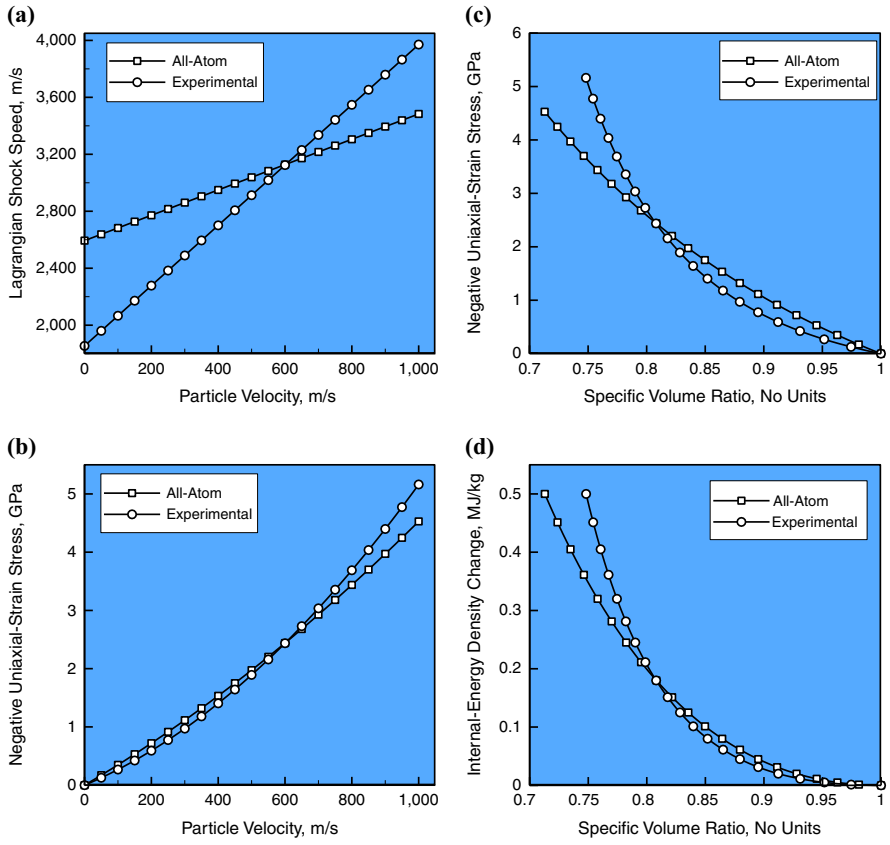

Figure 7.
All-atom molecular-level computational-analysis – and the experimental-analysis – (Mock *et al.*, 2009) based Hugoniot relations in polyurea

Notes: (a) Lagrangian shock speed, *Us* vs particle velocity, u_p; (b) (negative) longitudinal stress, $-t_{11}$ vs *up*; (c) $-t_{11}$ vs normalized specific volume, v/v_0 (v0 denotes the material initial specific volume); and (d) (mass-based) internal energy density, e vs v/v_0

noted that the procedure employed can yield only the Hugoniot relations which do not involve material thermal-state variables (e.g. temperature and entropy density). To determine Hugoniot relations which involve material thermal-state variables, an all-atom molecular-level computational procedure developed in our recent work (Grujicic *et al.*, 2011f) can be utilized.

Examination of Figure 7(a)-(d) reveals that the computational results are only in fair agreement with their experimental counterparts. This finding is not completely unexpected, considering the fact that the forcefield functions used in the present work were derived by fitting the quantum mechanical data for the configurational states which are not drastically different from the material reference state (the material state under standard ambient conditions). In sharp contrast, under shock-loading conditions, the material is placed into a state of large density, high internal stress and high temperatures. It is, hence, not very likely that the shocked material states were used during parameterization of the forcefield functions.

As mentioned earlier, the Hugoniot relations, such as those displayed in Figure 7(a)-(d), are generally used, within the continuum-material framework, in two ways:

(1) to conduct various planar longitudinal shock generation, propagation and interaction analyses (Grujicic *et al.*, 2012c); and

(2) to help derive and parameterize the appropriate continuum-type material constitutive models which capture material behavior under high-rate, large-strain, high-pressure loading conditions.

These models are subsequently used in general three-dimensional, transient non-linear dynamics computational analyses of various blast- and ballistics-related scenarios (e.g. Grujicic *et al.*, 2010b). As will be shown later, the Hugoniot relations in the present work are used to carry out a continuum-level analysis of the interaction of an incident shockwave with polyurea/glass and glass/polyurea material interfaces.

3.1.3 Shock-induced changes in the material microstructure. To assess the nature and the extent of microstructural changes induced in polyurea by the passage of an incident shockwave, the following four microstructural parameters are monitored:

(1) the extent of (relative) transverse motion of the atoms at the shockwave-front;

(2) the extent of covalent-bond breaking within the polyurea chains;

(3) the extent of breaking of the hydrogen bonds that are responsible for the formation of hard domains; and

(4) the degree of shockwave-induced permanent densification (density increase).

The results obtained can be summarized as follows:

(1) Relative transverse atomic displacements of magnitudes comparable with the shockwave-front width are observed in polyurea. Since these relatively large atomic displacements can induce inelastic deformation and changes in the nearest-neighbor atomic coordination in the material at the shockwave-front, they can be considered as potent energy-absorbing/shockwave-dispersive processes. In addition, generation of the transverse atomic displacements at the shock front is the key mechanism by which the system converts the uniaxial kinetic energy (brought into the system by the imposed axial contraction of the unit cell) into the thermal (i.e. three-dimensional kinetic) energy.

(2) While the force-field used in the present work enables covalent bond-breaking/formation, such intra-chain molecular-structure changes were not observed in polyurea. Thus, these processes are not expected to play any significant role in the energy dissipation and shockwave dispersion, within the shockwave-strength range explored in the present work.

(3) Typical changes in the hydrogen bond distribution caused by the passage of a shockwave are displayed in Figure 8(a)-(b). Figure 8(a) displays a zoomed-in view of the initial molecular-level configuration of a region within the hard domain of nano-segregated polyurea. Figure 8(b) shows the same region after the right-propagating shockwave has swept approximately one-third of this region. For improved clarity, covalent bonds are not displayed in Figure 8(a)-(b), while hydrogen bonds are shown as dashed lines. A comparison of the results displayed in Figure 8(a)-(b) reveals that the passage of the shockwave increases the total number of the hydrogen bonds. In this process some of the hydrogen

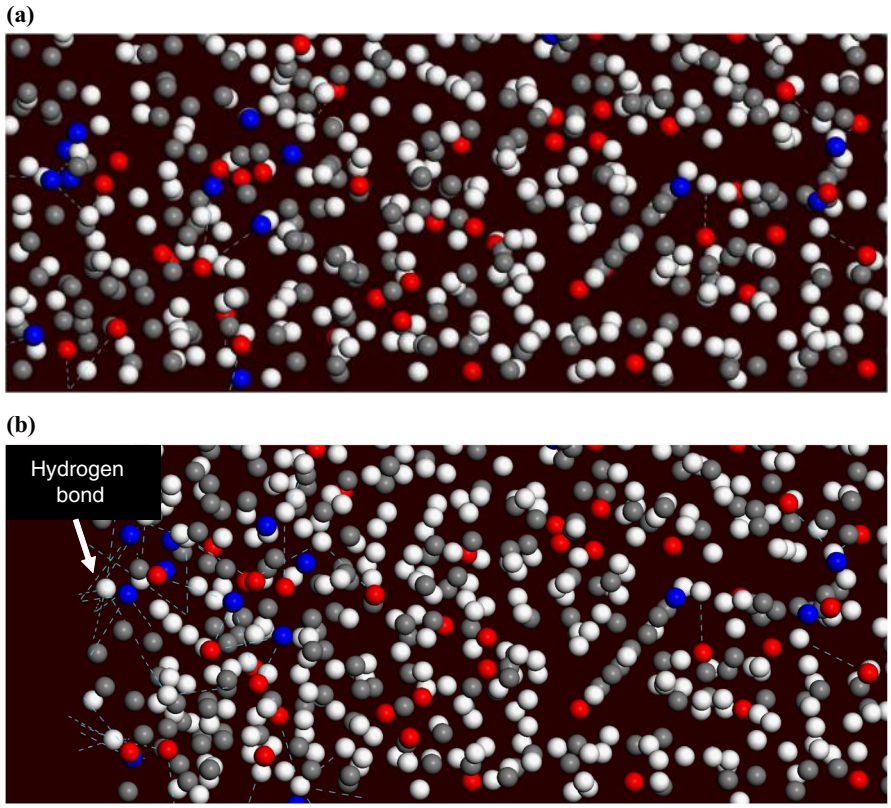

Figure 8.
A zoomed-in view of the molecular-level configuration of a region within the hard domain of polyurea

Notes: (a) Before; and (b) after the passage of a right-propagating shockwave. For improved clarity, covalent bonds are not shown, while the hydrogen bonds are depicted using dashed lines

bonds present in the initial configuration are eliminated, others survived, while many new hydrogen bonds have been created. Hydrogen-bond breaking/(re)building has been previously found to be a fairly potent shockwave-energy absorbing/dissipating mechanism (Grujicic *et al.*, 2012i).

(4) Passage of the shock has been found to cause a permanent (1-2 percent) increase in the material mass-density. By carefully examining the shocked-material molecular-level microstructure, it was found that the observed shock-induced permanent densification is mainly localized within the hard domains. In fact, passage of the shock through the hard domains, was found to increase the degree of order within these regions of the material. Material permanent densification process(es) are fully expected to contribute to shockwave-energy absorption/dissipation.

The discussion presented above suggests that large relative transverse displacements, hydrogen-bond breaking/rebuilding and permanent densification processes all contribute to the well-established ability of polyurea to mitigate resident-shock

effects. While, in the discussion given above, these processes were treated as being distinct, there is a high probability that the microstructural parameter monitored simply revealed different aspects of the same microstructural evolution process. Simply stated, transverse relative displacement of the atoms within the shockwave-front is accompanied by hydrogen-bond breaking/rebuilding and by material-ordering-induced permanent densification.

3.2 Soda-lime glass

In this subsection, the basic procedures and results related to: the generation and propagation of incident shockwaves in soda-lime glass; construction of the corresponding shock Hugoniot relations; and identification of the major shockwave-induced microstructural changes are presented and discussed.

3.2.1 Incident shockwave generation and propagation. Examples of the results, associated with a continuous axial contraction of the computational cell in soda-lime glass, are displayed in Figure 9(a)-(d). The generation and propagation of a pair of converging planar shockwaves is evident.

To reveal the structure/shape of the shockwave-front, the aforementioned method based on the use of Lagrangian bins was utilized. Two examples of the results obtained (for the right-propagating shockwave only) are shown in Figure 10(a)-(b), (for the

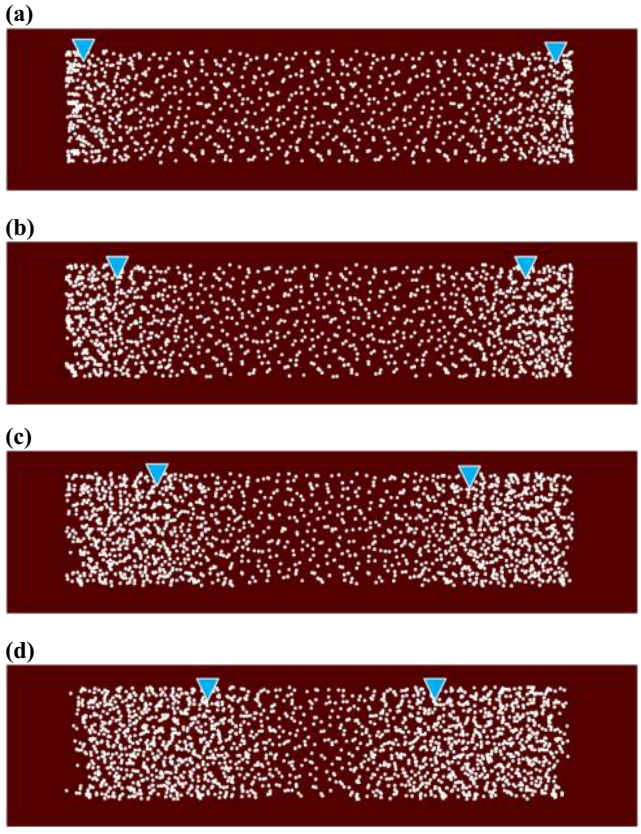

Figure 9.
Temporal evolution of the molecular-level material microstructure accompanying generation and propagation of a pair of converging planar shocks in glass

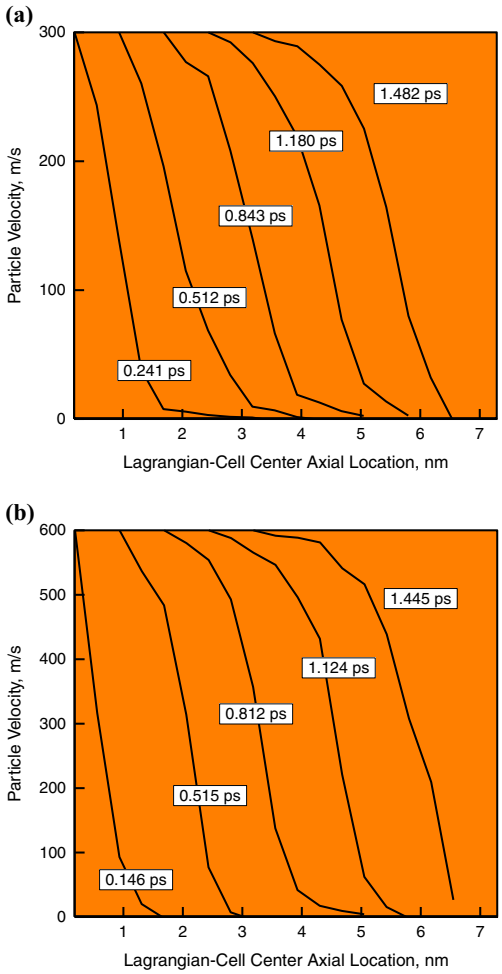

Figure 10.
Temporal evolution of the particle velocity associated with a right-propagating shockwave in glass under imposed (maximum) particle velocities

Notes: Curve labels pertain to the respective post-shock initiation times. (a) 300 m/s; (b) 600 m/s

imposed particle velocities of 300 and 600 m/s, respectively). Examination of the (particle velocity vs longitudinal position) results displayed in Figure 10(a)-(b) reveals establishment of steady shockwaves. Post-shock-generation times in ps are used as curve labels in Figure 10(a)-(b).

3.2.2 Determination of shock Hugoniot relations. The aforementioned shock-jump equation-based method was also applied to the soda-lime glass in order to determine the four (previously defined) shock Hugoniot relations. The results of this procedure are displayed in Figure 11(a)-(d). For comparison, experimental results of Alexander *et al.* (2008) are also shown in these figures. It is seen that, again, the agreement between the corresponding computational and experimental results is only fair. This finding also can be attributed to the potential shortcomings of the forcefields when used for the material in the highly shocked condition.

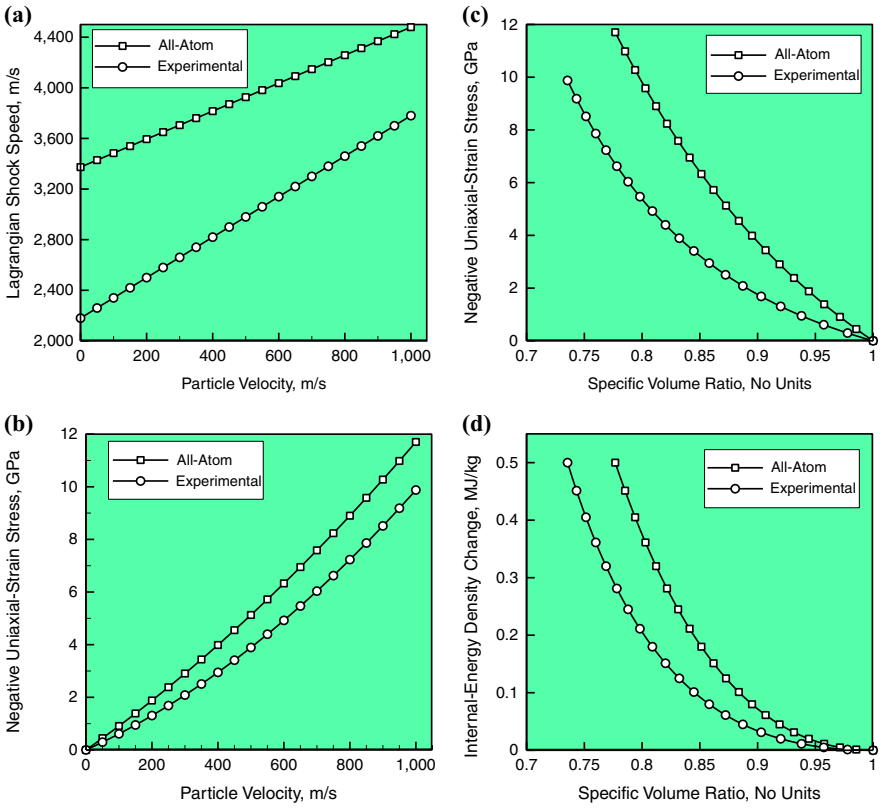

Notes: (a) Lagrangian shock speed, U_s vs particle velocity, u_p; (b) (negative) longitudinal stress, $-t_{11}$ vs u_p; (c) $-t_{11}$ vs normalized specific volume, v/v_0 (v_0 denotes the material initial specific volume); and (d) (mass-based) internal energy density, e vs v/v_0

Figure 11.
All-atom molecular-level computational-analysis – and the experimental-analysis – (Alexander *et al.*, 2008) based Hugoniot relations in glass

3.2.3 Shock-induced changes in the material microstructure. Shockwave-induced changes in two microstructural parameters are monitored in the case of soda-lime glass:

(1) the extent of lateral motion of the atoms at the shockwave-front; and

(2) the extent of changes to the Si and O atomic coordination (i.e. bonding structure).

In soda-lime glass, transverse displacements are observed with magnitudes smaller by approximately 30-50 percent than those observed in the polyurea case. Nevertheless, these displacements produce a permanent change in atomic nearest-neighbor coordination (as well as assisting in the permanent volume change of the shocked material). However, the amorphous nature of soda-lime glass precludes a more detailed/quantitative description of the nature of the atomic lateral-motion-induced inelastic-deformation process(es) or the associated microstructural defect formation. On the other hand, the accompanying changes in the atomic coordination and the bond structure can be readily identified (as will be demonstrated below).

Examples of the shock-loading-induced changes in the atomic coordination and bond structure of soda-lime glass are given in Figure 12(a)-(d). To aid in visualization/interpretation of the microstructural/topological changes experienced by soda-lime glass during shock loading, only a 20-30 atom exemplary region of the upstream material is analyzed in these figures. In addition, sodium cations are not displayed. It should be noted that the same color coding scheme for atomic species is used, as was shown in Figure 3. In Figure 12(a) and (c), *x-y* and *y-z* projections are given of the material region under consideration in its initial state. The corresponding projections for the same material region after the passing of a shock are displayed in Figure 12(b) and (d). A closer examination of the microstructure/topology results displayed in Figure 12(a)-(d) provides clear evidence for the formation of fivefold coordinated silicon atoms (highlighted in cyan for improved clarity). In addition, a comparison of the results displayed in Figure 12(a)-(b)

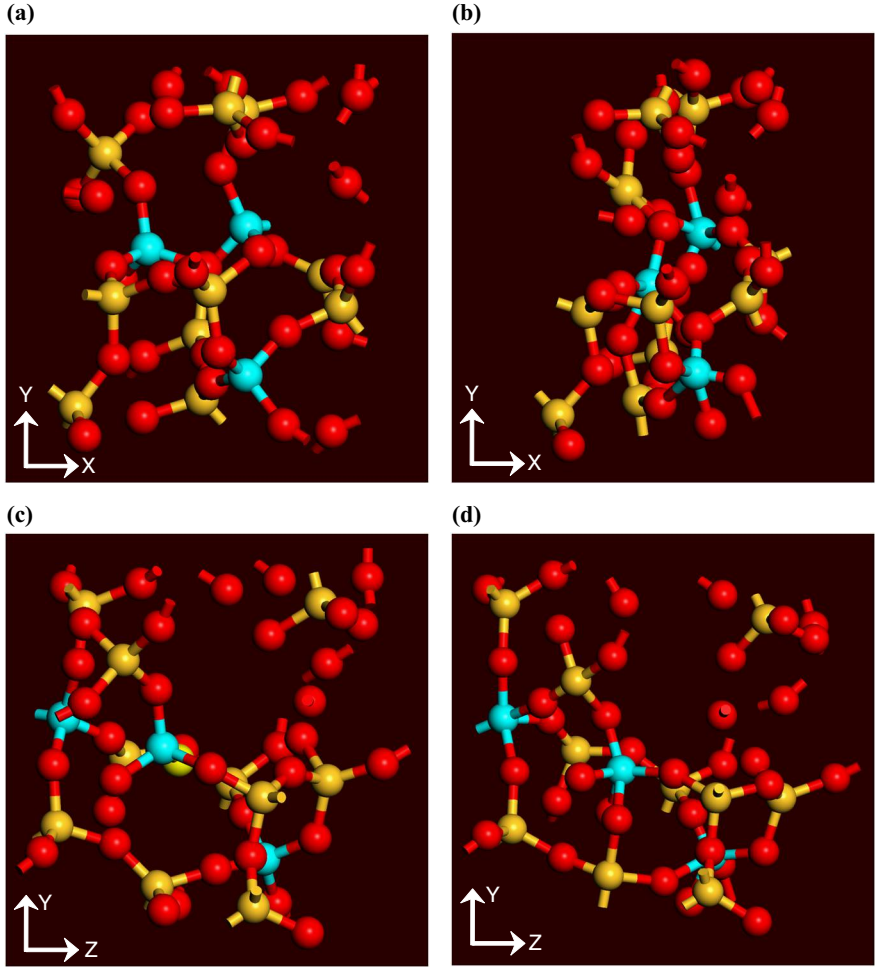

Figure 12.
Development of fivefold coordinated silicon atoms in soda-lime glass under shock loading

Notes: (a) Material initial state, *x-y* projection; (b) post-shock state of the same material region as in (a); (c) and (d) correspond respectively to the *y-z* projection of (a) and (b)

reveals the extent of (partly irreversible) compaction caused by shock-loading of soda-lime glass. Additional changes in the soda-lime molecular-level microstructure were also observed (the results not shown for brevity). For example, clear evidence was found that shockwave-loading produces smaller Si-O rings.

It should be noted that the molecular-level microstructural changes described above are a manifestation of the transition of soda-lime glass to a state that is energetically favored at high shock-induced stresses (large densities). This finding is consistent with the experimental observation of Alexander *et al.* (2008) who reported the formation of stishovite-like domains containing sixfold coordinated silicon atoms in soda-lime glass at ca. 30 GPa shock-induced axial stress levels. It should be noted that the maximum pressure experienced by glass during shock-loading in the present work was smaller by a factor of 3-4, than the maximum pressure experienced by glass in the work of Alexander *et al.* (2008). This difference can be used to account for the fact that no sixfold coordinated silicon was found in the present work.

It should be also recognized that shock loading leads to a permanent 2-4 percent (shock strength-dependent) increase in the material density. This material densification process along with the aforementioned processes leading to an increase in the silicon-atom coordination and smaller Si-O ring formation are all associated with energy absorption/dissipation.

3.3 Polyurea/glass material interface

In this subsection, the results pertaining to the interaction of an incident polyurea-resident shockwave with a polyurea/glass boundary are presented and discussed. The specific results addressed include: first, the use of the Hugoniot-based impedance-matching method to predict the outcome of the incident-shockwave interaction with the material boundary; second, direct molecular-level simulation of the outcome of the same interaction; and third, microstructural changes experienced by the polyurea/glass interfacial region as a result of the interaction of the incident polyurea-resident shockwave with the polyurea/glass interface.

3.3.1 Application of the impedance-matching method. Before the molecular-level computational results pertaining to the interaction of the incident polyurea-resident shockwave with the polyurea/glass interface are presented and discussed, the so-called impedance-matching method used to predict the outcome of such interaction (at the continuum-level) is overviewed. To explain this method, negative-stress, $-t_{11}$, vs particle velocity, u_p, Hugoniot relations are utilized. This type of Hugoniot relation is used since the interaction of a shockwave with the material boundary results in the formation of a transmitted shockwave and a reflected shock- or release-wave, while ensuring that the stress and the particle velocities remain continuous across the material boundary. To help explain the impedance-matching method, $-t_{11}$ vs u_p Hugoniot relations for polyurea and soda-lime glass are depicted (using solid lines) in Figure 13(a). The states of the (shocked) polyurea and the stress-free quiescent glass material, before the right-propagating shockwave interacts with the polyurea/glass interface, are denoted by a filled square (labeled A) and triangle (labeled B), respectively. After the interaction of the incident shockwave with the material interface, the state of the adjoining materials swept by their transmitted/reflected waves is obtained by:

(1) Mirroring the polyurea Hugoniot about a vertical constant-u_{p} line with the value of u_{p} corresponding to that associated with the incident polyurea-resident shockwave. The result of this exercise is depicted in Figure 13(a) using a dashed line; and

(2) The intersection of the mirrored polyurea Hugoniot with the glass Hugoniot defines the states of the two materials swept by their respective transmitted/reflected waves, point C in Figure 13(a).

A comparison of the material states corresponding to point C with those corresponding to the material states A and B and the orientation of the polyurea and glass $-t_{11}$ vs u_p Hugoniots passing through point C reveal that: a right-propagating transmitted shockwave is generated in the glass; and a left-propagating reflected shockwave is generated in the polyurea. It is the fact that the magnitude of $-t_{11}$ increases in the two materials as a result of the interaction of the incident shockwave with the material

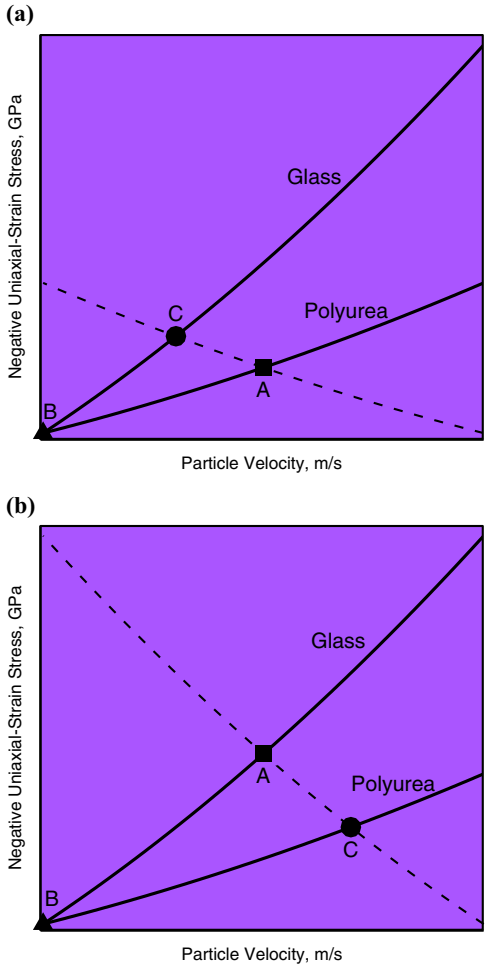

Figure 13.
Impedance-matching procedure used to determine the outcome of the interaction of an incident shockwave

Notes: (a) polyurea with the polyurea/glass interface; and (b) soda-line glass with the glass/polyurea interface. Please see text for explanation of the labeled points and dashed lines

boundary, that defines the shockwave character of the transmitted and reflected waves. Also, since the polyurea is re-shocked by a left-propagating wave, there is an accompanying decrease in the (positive) value of u_p.

Application of the procedure described above, and the use of the previously mentioned shock-jump equations, to the problem of interaction of an incident shockwave within polyurea with the polyurea/glass interface, is shown in Figure 14(a)-(f). It should be noted that only the all-atom molecular-level computation-based Hugoniot relations are used in this portion of the work. In other words, polyurea and soda-lime glass are treated as continuum materials with the shock-Hugoniot relations corresponding to the ones obtained using the all-atom molecular-level computations. Since polyurea and soda-lime glass are treated as continuum materials, the resident shock/release waves are considered as being of a discontinuous nature, i.e. with zero width.

In Figure 14, parts (a), (c) and (e) correspond to the state of the polyurea/glass bi-material before the interaction, while parts (b), (d) and (f) correspond to the state of the same bi-material after the interaction. Three state/kinematic variables are monitored in these figures:

(1) particle velocity;

(2) negative stress; and

(3) mass density.

Application of the impedance-matching method and the use of the all-atom molecular-level computation-based Hugoniot relations for polyurea and soda-lime glass yielded the results labeled "Hugoniot-based" in Figure 14(a)-(f). Examination of these results reveals that the interaction of an incident polyurea-resident shockwave with the polyurea/glass boundary: first, creates a transmitted right-propagating shockwave which imparts positive particle velocity and compressive stress to, while increasing the mass density of, the "shocked" glass; and second, creates a reflected left-propagating shockwave which further decreases the particle velocity, increases the compressive stress and increases the mass density of the "re-shocked" polyurea.

3.3.2 Molecular-level simulation results of the shockwave/material-boundary interaction. It should be recalled that in the case of the results labeled "Hugoniot-based" in Figure 14(a)-(f), the impedance-matching method was used, in conjunction with the all-atom Hugoniot relations and shock-jump equations to determine the condition of continuous stress and particle velocity (as well as the discontinuity in the material density) across the polyurea/glass interface. In this section, the impedance-matching method was not used. Instead, the previously mentioned Lagrangian-bin method was used in conjunction with the molecular simulation results in order to determine the continuous particle-velocity across the polyurea/glass interface. In addition, the virial theorem (Grujicic *et al.*, 2013a) was used to determine the continuous axial-stress condition, while the local particle number-density was used to compute the corresponding mass-density discontinuity condition, across the same interface. The results of this procedure (labeled as "Simulation-based") are also depicted in Figure 14(a)-(f).

A comparison of the corresponding "Hugoniot-based" and "Simulation-based" results displayed in Figure 14(a)-(f) reveals:

(1) Before the interaction of the incident polyurea-resident shockwave with the polyurea/glass interface, the location of the shock front and the upstream particle velocities are identical for the two sets of results, Figure 14(a). This finding is consistent with the fact that the same set of U_s vs u_p results obtained

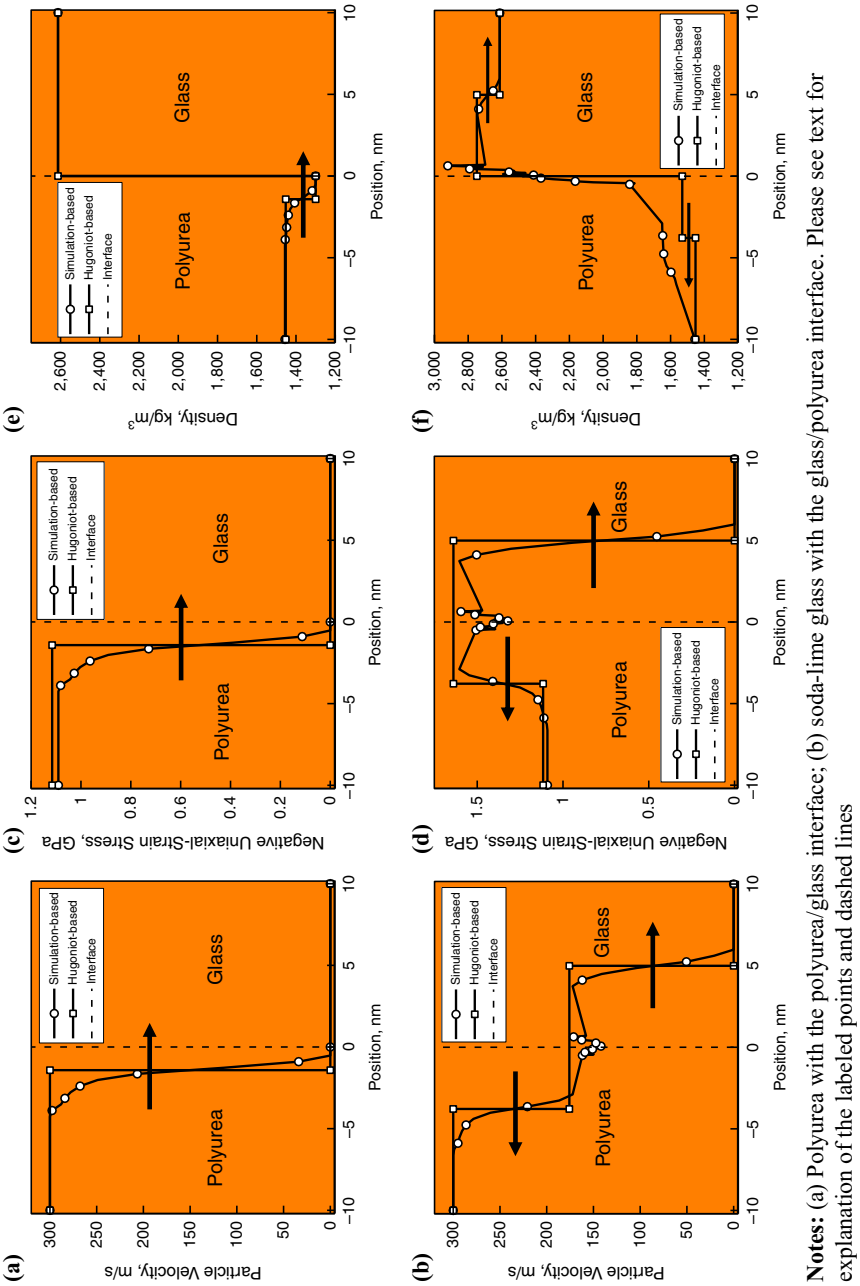

Figure 14.
Distribution of the particle velocity, (a)-(b), negative axial stress, (c)-(d) and mass density, (e)-(f) along the length of the polyurea/glass bi-material before, (a), (c), (e) and after, (b), (d), (f) the interaction of the incident shockwave residing in polyurea with the polyurea/glass boundary

Notes: (a) Polyurea with the polyurea/glass interface; (b) soda-lime glass with the glass/polyurea interface. Please see text for explanation of the labeled points and dashed lines

through the use of all-atom molecular-level computations was utilized to generate the two sets of results. The only difference between the two sets of results is that in the case of the "Simulation-based" results, the shock front has a finite width.

(2) The two sets of results agree fairly well with respect to the level of the negative stress, Figure 14(c), and the mass density, Figure 14(e), attained in the portion of polyurea swept by the incident shock. Again, as expected, the "Hugoniot-based" results pertain to a discontinuous shockwave while the "Simulation-based" results account for the final width of the shockwave front.

(3) As in the case of the "Hugoniot-based" results, the "Simulation-based" results show the formation of a transmitted right-propagating shockwave and a reflected left-propagating shockwave upon the interaction of the incident polyurea-resident shockwave with the polyurea/glass interface. However, the two sets of results considered show more differences than in the case of the incident shock. Specifically: the velocities of the transmitted and reflected shockwaves differ for the two sets of results; while continuity in the particle velocity and stress appears to be maintained in the case of the "Simulation-based" results, these results are quite irregular in the interfacial region. Further away from the interfacial region, the "Simulation-based" results tend to reacquire their "well-behaved" character. These findings suggest that, perhaps, the polyurea/glass interfacial region may undergo shock-induced microstructural changes resulting in the formation of a polyurea/glass interphase.

3.3.3 Shock-induced changes in the material-boundary microstructure. The results presented in the previous section suggested the possibility of the formation of a shock-induced polyurea/glass interphase. In this section, the results pertaining to the examination of the material microstructure in the polyurea/glass interfacial region are presented and discussed. Figure 15(a) shows a relatively thin slice of the "pre-shocked" molecular structure of the polyurea/glass bi-material. Examination of this figure reveals the presence of: a fairly flat and "clean" polyurea/glass interface; and hydrogen bonding (depicted using dashed lines) within the hard domains of the polyurea (revealed by their blue-colored nitrogen-constituents). The same interfacial region following the interaction of the incident polyurea-resident shockwave within the polyurea/glass interface is depicted in Figure 15(b). Careful examination of the molecular structure displayed in this figure reveals the presence of a thin interface region characterized by: an irregular interface indicating interpenetration and mechanical interlocking of the two adjoining materials; and a higher concentration of hydrogen bonds and the establishment of hydrogen bonds between hydrogen residing in polyurea and oxygen residing in glass. The presence of this interphase region can then be used to explain the aforementioned differences between the "Hugoniot-based" and "Simulation-based" results in the interfacial region, as observed in Figure 14(b), (d) and (f).

To quantify the extent of microstructural changes induced by the interaction of the polyurea-resident shockwave with polyurea and with the polyurea/glass interface, pair-correlation and coordination-number analyses were carried out using the procedures described in our prior work (Grujicic *et al.*, 2012g). The results obtained can be summarized as follows:

(1) Pre-shocked materials: polyurea – the highest-probability N-N distance in hard domains = 0.365 nm, N-N coordination number within hard domains = 7.55; and glass – the highest-probability Si-O, Si-Si and O-O distances = 0.180, 0.300 and 0.260 nm respectively, Si and O atom coordination numbers = 4.05 and 2.01, respectively.

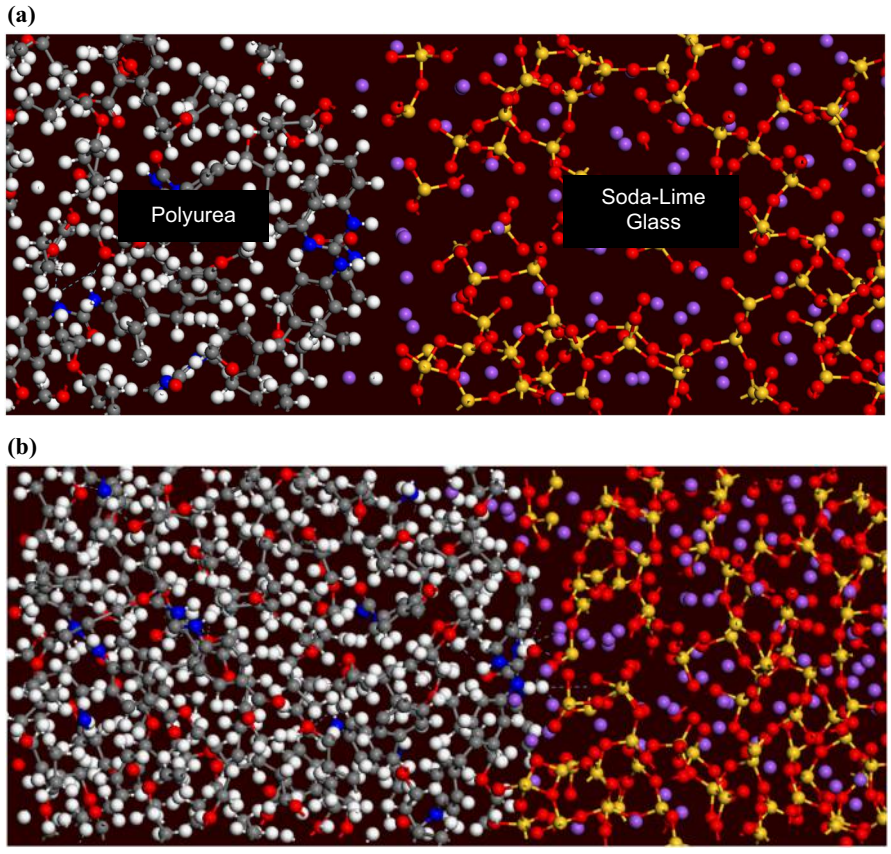

Figure 15.
Molecular-level microstructure of the polyurea/glass interfacial region

Notes: (a) Before; (b) after the interaction of the incident polyurea-resident shockwave with the interface

(2) Shocked materials far from the interface: polyurea – the highest-probability N-N distance in hard domains = 0.350 nm, N-N coordination number within hard domains = 7.78; and glass – the highest-probability Si-O, Si-Si and O-O distances = 0.178, 0.297 and 0.257 nm, respectively, Si and O atom coordination numbers = 4.10 and 2.03, respectively.

(3) Shocked materials adjacent to the interface: polyurea – the highest-probability N-N distance in hard domains = 0.329 nm, N-N coordination number within hard domains = 8.17; and glass – the highest-probability Si-O, Si-Si and O-O distances = 0.174, 0.291 and 0.252 nm, respectively, Si and O atom coordination numbers = 4.51 and 2.23, respectively.

These results clearly show that the passage of the incident shockwave causes microstructural changes within polyurea and even larger changes in the two phases adjacent to the polyurea/glass interface, while the transmitted shockwave causes changes in glass.

3.4 Glass/polyurea material interface

In this subsection, the results pertaining to the interaction of an incident glass-resident shockwave with a glass/polyurea boundary are presented and discussed. The specific results addressed include: the use of the Hugoniot-based impedance-matching method to predict the outcome of the incident-shockwave interaction with the material boundary; direct molecular-level simulation of the outcome of the same interaction; and microstructural changes experienced by the glass/polyurea interfacial region as a result of the interaction of the incident glass-resident shockwave with the glass/polyurea interface.

3.4.1 Application of the impedance-matching method. The previously mentioned impedance-matching method is also utilized in this case. In this case, $-t_{11}$ vs u_p Hugoniot relations for polyurea and soda-lime glass are depicted (using solid lines) in Figure 13(b). The states of the (shocked) soda-lime glass and the stress-free quiescent polyurea material, before the right-propagating shockwave interacts with the glass/polyurea interface, are denoted by a filled square (labeled A) and triangle (labeled B), respectively. After the interaction of the incident shockwave with the material interface, the state of the adjoining materials swept by their transmitted/reflected waves is obtained by:

(1) Mirroring the glass Hugoniot about a vertical constant-u_{p} line with the value of u_{p} corresponding to that associated with the incident glass-resident shock. The result of this exercise is depicted in Figure 13(b) using a dashed line.

(2) The intersection of the mirrored glass Hugoniot with the polyurea Hugoniot defines the states of the two materials swept by their respective transmitted/reflected waves, point C in Figure 13(b).

A comparison of the material states corresponding to point C with those corresponding to the material states A and B and the orientation of the polyurea and glass $-t_{11}$ vs u_p Hugoniots passing through point C reveal that: a right-propagating transmitted shockwave is generated in the polyurea; and a left-propagating reflected release-wave is generated in the glass. It is the fact that the magnitude of $-t_{11}$ decreases in the glass as a result of the interaction of the incident shockwave with the material boundary, that defines the release-wave character of the reflected wave. Also, since the pre-shocked glass is relaxed by the passage of the release-wave, there is an accompanying increase in the (positive) value of u_p in this material.

Application of the procedure described above, and the use of the previously mentioned shock-jump equations, to the problem of interaction of an incident shockwave within glass, with the glass/polyurea interface, is shown in Figure 16(a)-(f). It should be recalled that only the all-atom molecular-level computation-based Hugoniot relations are used in this portion of the work and the results obtained are labeled as "Hugoniot-based."

In Figure 16, parts (a), (c) and (e) correspond to the state of the glass/polyurea bi-material before the interaction, while parts (b), (d) and (f) correspond to the state of the same bi-material after the interaction. The same three state/kinematic variables, as in the case of Figure 14(a)-(f), are monitored in Figure 16(a)-(f).

Examination of the results labeled "Hugoniot-based" in Figure 16(a)-(f) reveals that the interaction of an incident glass-resident shockwave with the glass/polyurea boundary: first, creates a transmitted right-propagating shockwave which imparts positive particle velocity and compressive stress to, while increasing the mass density

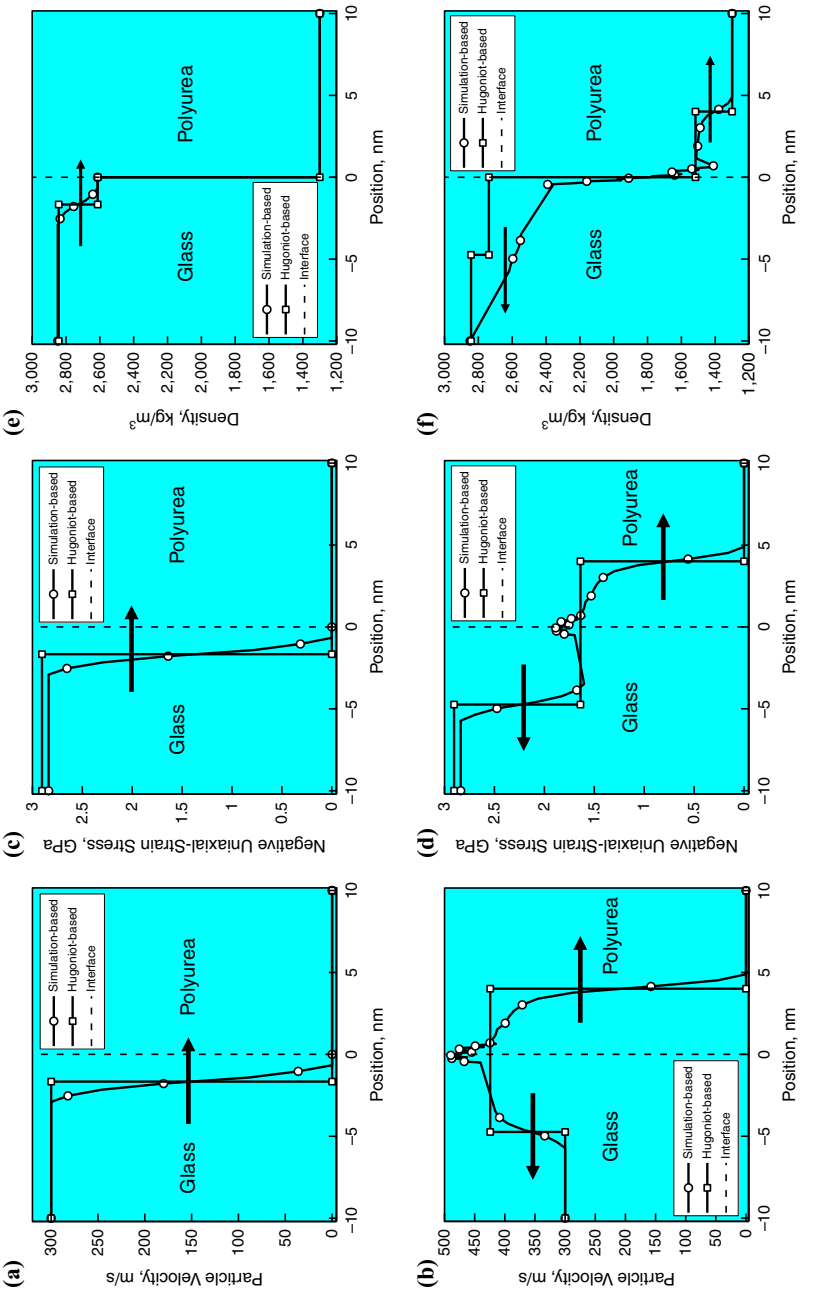

Figure 16.
Distribution of the particle velocity, (a)-(b), negative axial stress, (c)-(d) and mass density, (e)-(f) along the length of the glass/polyurea bi-material before, (a), (c), (e) and after, (b), (d), (f) the interaction of the incident shockwave residing in glass with the glass/polyurea boundary

of, the "shocked" polyurea; and second, creates a reflected left-propagating release wave which increases the particle velocity, decreases the compressive stress and decreases the mass density of the swept material.

3.4.2 Molecular-level simulation results of the shockwave/material-boundary interaction. The results obtained in this portion of the work (labeled as "Simulation-based" in Figure 16(a)-(f)) are again obtained by combining the Lagrangian-bin method with the virial theorem and the method for determination of the particle number-density.

A comparison of the corresponding "Hugoniot-based" and "Simulation-based" results displayed in Figure 16(a)-(f) reveals that:

(1) Before the interaction of the incident glass-resident shockwave with the glass/polyurea interface, the location of the shock front and the upstream particle velocities are identical for the two sets of results, Figure 16(a). This finding is consistent with the fact that the same set of U_s vs u_p results obtained through the use of all-atom molecular-level computations was utilized to generate the two sets of results. The only difference between the two sets of results is that, again, in the case of the "Simulation-based" results, the shock front has a finite width.

(2) The two sets of results agree fairly well with respect to the level of the negative stress, Figure 16(c), and the mass density, Figure 16(e), attained in the portion of glass swept by the incident shock. Again, as expected, the "Hugoniot-based" results pertain to a discontinuous shockwave while the "Simulation-based" results account for the final width of the shockwave front.

(3) As in the case of the "Hugoniot-based" results, the "Simulation-based" results show the formation of a transmitted right-propagating shockwave and a reflected left-propagating release-wave upon the interaction of the incident glass-resident shockwave with the glass/polyurea interface. However, the two sets of results considered again show more differences than in the case of the incident shock. Specifically: the velocities of the transmitted shockwave and reflected release-wave differ for the two sets of results; while continuity in the particle velocity and stress appears to be maintained in the case of the "Simulation-based" results, these results are somewhat irregular in the interfacial region. Further away from the interfacial region, the "Simulation-based" results tend to reacquire their "well-behaved" character. These findings once more suggest that the glass/polyurea interfacial region may undergo shock-induced microstructural changes resulting in the formation of a glass/polyurea interphase.

3.4.3 Shock-induced changes in the material-boundary microstructure. The results presented in the previous section suggested the possibility of the formation of a shock-induced glass/polyurea interphase. In this section, the results pertaining to the examination of the material microstructure in the glass/polyurea interfacial region are presented and discussed. Figure 17(a) shows a relatively thin slice of the "pre-shocked" molecular structure of the glass/polyurea bi-material. Examination of this figure reveals the presence of: a fairly flat and "clean" glass/polyurea interface; and hydrogen bonding (depicted using dashed lines) within the hard domains of the polyurea (revealed by their blue-colored nitrogen-constituents). The same interfacial region following the interaction of the incident glass-resident shockwave within the glass/polyurea interface is depicted in Figure 17(b). Careful examination of the molecular structure displayed in this figure again reveals the presence of a thin

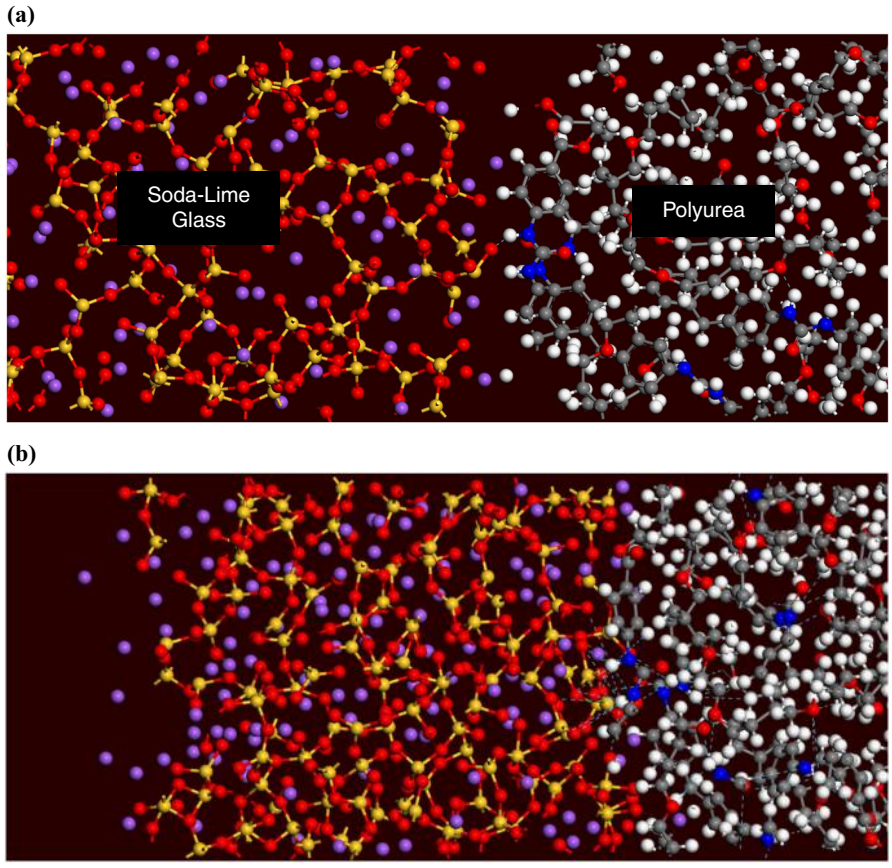

Figure 17.
Molecular-level microstructure of the glass/polyurea interfacial region

Notes: (a) Before; (b) after the interaction of the incident glass-resident shockwave with the interface

interface region characterized by: first, an irregular interface indicating interpenetration and mechanical interlocking of the two adjoining materials; and second, a higher concentration of hydrogen bonds and the establishment of hydrogen bonds between hydrogen residing in polyurea and oxygen residing in glass. The presence of this interphase region can again be used to explain the aforementioned differences between the "Hugoniot-based" and "Simulation-based" results in the interfacial region, as observed in Figure 16(b), (d) and (f).

To quantify the extent of microstructural changes induced by the interaction of the glass-resident shockwave with glass and with the glass/polyurea interface, pair-correlation and coordination-number analyses were carried out using the procedures mentioned earlier. The results obtained can be summarized as follows:

(1) Pre-shocked materials: glass – the highest-probability Si-O, Si-Si and O-O distances = 0.180, 0.300 and 0.260 nm, respectively, Si and O atom coordination numbers = 4.05 and 2.01, respectively; and polyurea – the highest-probability N-N distance in hard domains = 0.365 nm, N-N coordination number within hard domains = 7.55.

(2) Shocked materials far from the interface: glass – the highest-probability Si-O, Si-Si and O-O distances = 0.179, 0.299 and 0.259 nm, respectively, Si and O atom coordination numbers = 4.07 and 2.02, respectively; and polyurea – the highest-probability N-N distance in hard domains = 0.358 nm, N-N coordination number within hard domains = 7.66.

(3) Shocked materials adjacent to the interface: glass – the highest-probability Si-O, Si-Si and O-O distances = 0.178, 0.298 and 0.257 nm, respectively, Si and O atom coordination numbers = 4.09 and 2.03, respectively; and polyurea – the highest-probability N-N distance in hard domains = 0.354 nm, N-N coordination number within hard domains = 7.55.

These results clearly show that the passage of the incident shockwave causes microstructural changes within glass and even larger changes in the two phases adjacent to the glass/polyurea interface, while the transmitted shockwave causes changes in polyurea. It should be noted that, in accordance with the results displayed in Figure 14(a)-(f) and Figure 16(a)-(f), the extent of microstructural changes after the reflection of the incident shock from the interface is larger in the case of polyurea-resident than in the case of the glass-resident incident shockwave.

4. Summary and conclusions

Based on the results obtained in the present work, the following summary remarks and main conclusions can be drawn:

(1) Molecular-level computational methods and tools are used to analyze propagation of shockwaves in polyurea and soda-lime glass, and their interactions with the polyurea/glass and glass/polyurea material interfaces.

(2) The results related to the propagation of the shockwaves within polyurea and glass are used to construct the corresponding shock-Hugoniot relationships, which were subsequently compared with their experimental counterparts. The agreement obtained was only fair, suggesting potential limitations of the force-fields when they are used in the high-pressure simulations.

(3) Propagation of sufficiently strong shockwaves through polyurea or glass has been found to cause microstructural changes, which play an important role in the process of absorption/dissipation of the energy carried by the shockwaves.

(4) In the case of the interaction of shockwaves with the polyurea/glass and glass/polyurea interfaces, it was found that the interfacial region undergoes additional microstructural changes leading to the formation of a polyurea/glass interphase. The formation of such an interphase has been found to alter the characteristics of the transmitted shockwaves and the reflected shock-/release-waves at the material interfaces in question.

References

Alexander, C.S., Chhabildas, L.C., Reinhart, W.D. and Templeton, D.W. (2008), "Changes to the shock response of fused quartz due to glass modification", *International Journal of Impact Engineering*, Vol. 35 No. 12, pp. 1376-1385.

Amirkhizi, A.V., Isaacs, J., McGee, J. and Nemat-Nasser, S. (2006), "An experimentally-based viscoelastic constitutive model for polyurea, including pressure and temperature effects", *Philosophical Magazine*, Vol. 86 No. 36, pp. 5847-5866.

Bogoslovov, R.B., Roland, C.M. and Gamache, R.M. (2007), "Impact-induced glass transition in elastomeric coatings", *Applied Physics Letters*, Vol. 90 No. 22, pp. 221910-1-221910-3.

Castagna, A.M., Pangon, A., Choi, T., Dillon, G.P. and Runt, J. (2012), "The role of soft segment molecular weight on microphase separation and dynamics of bulk polymerized polyureas", *Macromolecules*, Vol. 45 No. 20, pp. 8438-8444.

Davison, L. (2008), *Fundamentals of Shock Wave Propagation in Solids*, Springer-Verlag, Berlin.

Grujicic, M. and Lai, S.G. (1999), "Kinetic Monte Carlo modeling of chemical vapor deposition of (111) oriented diamond film", *Journal of Materials Science*, Vol. 34 No. 1, pp. 7-20.

Grujicic, M. and Pandurangan, B. (2012), "Meso-scale analysis of segmental dynamics in micro-phase segregated polyurea", *Journal of Materials Science*, Vol. 47, pp. 3876-3889.

Grujicic, M., He, T. and Pandurangan, B. (2011a), "Development and parameterization of an equilibrium material model for segmented polyurea", *Multidiscipline Modeling in Materials and Structures*, Vol. 7 No. 4, pp. 96-114.

Grujicic, M., Bell, W.C., Pandurangan, B. and He, T. (2010a), "Blast-wave impact-mitigation capability of polyurea when used as helmet suspension pad material", *Materials and Design*, Vol. 31, pp. 4050-4065.

Grujicic, M., Bell, W.C., Pandurangan, B. and Glomski, P.S. (2011b), "Fluid/structure interaction computational investigation of the blast-wave mitigation efficacy of the advanced combat helmet", *Journal of Materials Engineering and Performance*, Vol. 20 No. 1, pp. 877-893.

Grujicic, M., Pandurangan, B., Bell, W.C. and Bagheri, S. (2012b), "Shock-wave attenuation and energy-dissipation potential of granular materials", *Journal of Materials Engineering and Performance*, Vol. 21 No. 6, pp. 167-179.

Grujicic, M., Snipes, J.S., Galgalikar, R. and Ramaswami, S. (2014a), "Material-model based determination of the Shock-Hugoniot relations in nanosegregated polyurea", *Journal of Materials Engineering and Performance*, Vol. 23 No. 1, pp. 357-371.

Grujicic, M., Marvi, H., Arakere, G., Bell, W.C. and Haque, I. (2010b), "The effect of up-armoring the high-mobility multi-purpose wheeled vehicle (HMMWV) on the off-road vehicle performance", *Multidiscipline Modeling in Materials and Structures*, Vol. 6 Nos 29/30, pp. 229-256.

Grujicic, M., Snipes, J.S., Ramaswami, S., Yavari, R. and Ramasubramanian, M.K. (2014b), "Meso-scale computational investigation of shock-wave attenuation by trailing release-wave in different grades of polyurea", *Journal of Materials Engineering and Performance*, Vol. 23 No. 2, pp. 49-64.

Grujicic, M., Pandurangan, B., He, T., Cheeseman, B.A., Yen, C.-F. and Randow, C.L. (2010c), "Computational investigation of impact energy absorption capability of polyurea coatings via deformation-induced glass transition", *Materials Science and Engineering A*, Vol. 527 No. 2, pp. 7741-7751.

Grujicic, M., Pandurangan, B., King, A.E., Runt, J., Tarter, J. and Dillon, G. (2011c), "Multi-length scale modeling and analysis of microstructure evolution and mechanical properties in polyurea", *Journal of Materials Science*, Vol. 46 No. 6, pp. 1767-1779.

Grujicic, M., He, T., Pandurangan, B., Svingala, F.R., Settles, G.S. and Hargather, M.J. (2011d), "Experimental characterization and material-model development for microphase-segregated polyurea: an overview", *Journal of Materials Engineering and Performance*, Vol. 21 No. 7, pp. 2-16.

Grujicic, M., He, T., Pandurangan, B., Runt, J., Tarter, J. and Dillon, G. (2011e), "Development and parameterization of a time-invariant (equilibrium) material model for segmented elastomeric polyureas", *Journal of Materials: Design and Applications*, Vol. 225 No. 6, pp. 182-194.

Grujicic, M., Pandurangan, B., Bell, W.C., Cheeseman, B.A., Yen, C.-F. and Randow, C.L. (2011f), "Molecular-level simulations of shock generation and propagation in polyurea", *Materials Science and Engineering A*, Vol. 528 Nos 10/11, pp. 3799-3808.

Grujicic, M., Bell, W.C., Pandurangan, B., Cheeseman, B.A., Patel, P. and Gazonas, G.A. (2012c), "Inclusion of material nonlinearity and inelasticity into a continuum-level material model for soda-lime glass", *Journal of Materials and Design*, Vol. 35 No. 8, pp. 144-155.

Grujicic, M., Bell, W.C., Pandurangan, B., Cheeseman, B.A., Fountzoulas, C. and Patel, P. (2012d), "Molecular-level simulations of shock generation and propagation in soda-lime glass", *Journal of Materials Engineering and Performance*, Vol. 21 No. 8, pp. 1580-1590.

Grujicic, M., d'Entremont, B.P., Pandurangan, B., Runt, J., Tarter, J. and Dillon, G. (2012e), "Concept-level analysis and design of polyurea for enhanced blast-mitigation performance", *Journal of Materials Engineering and Performance*, Vol. 21 No. 10, pp. 2024-2037.

Grujicic, M., Arakere, A., Pandurangan, B., Grujicic, A., Littlestone, A.A. and Barsoum, R.S. (2012f), "Computational investigation of shock-mitigation efficacy of polyurea when used in a combat helmet: a core sample analysis", *Multidiscipline Modeling in Materials and Structures*, Vol. 8 No. 23, pp. 297-331.

Grujicic, M., Ramaswami, S., Snipes, J.S., Yavari, R., Yen, C.-F. and Cheeseman, B.A. (2013a), "Axial-compressive behavior, including kink-band formation and propagation, of single p-phenylene terephthalamide (PPTA) fibers", *Advances in Materials Science and Engineering*, No. 7, Article ID 329549.

Grujicic, M., Pandurangan, B., Zhang, Z., Bell, W.C., Gazonas, G.A., Patel, P. and Cheeseman, B.A. (2012g), "Molecular-level analysis of shock-wave physics and derivation of the Hugoniot relations for fused silica", *Journal of Materials Engineering and Performance*, Vol. 21 No. 2, pp. 823-836.

Grujicic, A., LaBerge, M., Grujicic, M., Pandurangan, B., Runt, J., Tarter, J. and Dillon, G. (2012h), "Potential improvements in shock-mitigation efficacy of a polyurea-augmented advanced combat helmet: a computational investigation", *Journal of Materials Engineering and Performance*, Vol. 21 No. 3, pp. 1562-1579.

Grujicic, M., Yavari, R., Snipes, J.S., Ramaswami, S., Runt, J., Tarter, J. and Dillon, G. (2012i), "Molecular-level computational investigation of shock-wave mitigation capability of polyurea", *Journal of Materials Science*, Vol. 47 No. 2, pp. 8197-8215.

Grujicic, M., Snipes, J.S., Ramaswami, S., Yavari, R., Runt, J., Tarter, J. and Dillon, G. (2013b), "Coarse-grained molecular-level analysis of polyurea properties and shock-mitigation potential", *Journal of Materials Engineering and Performance*, Vol. 22, pp. 1964-1981.

Grujicic, M., Bell, W.C., Pandurangan, B., Cheeseman, B.A., Fountzoulas, C., Patel, P., Templeton, D.W. and Bishnoi, K.D. (2011g), "The effect of high-pressure densification on ballistic-penetration resistance of a soda-lime glass", *Journal of Materials: Design and Applications*, Vol. 225 No. 2, pp. 298-315.

Grujicic, M., d'Entremont, B.P., Pandurangan, B., Grujicic, A., LaBerge, M., Runt, J., Tarter, J. and Dillon, G. (2012j), "A study of the blast-induced brain white-matter damage and the associated diffuse axonal injury", *Multidiscipline Modeling in Materials and Structures*, Vol. 8 No. 8, pp. 213-245.

Grujicic, M., Bell, W.C., Glomski, P.S., Pandurangan, B., Cheeseman, B.A., Fountzoulas, C., Patel, P., Templeton, D.W. and Bishnoi, K.D. (2011h), "Multi-length scale modeling of high-pressure induced phase transformations in soda-lime glass", *Journal of Materials Engineering and Performance*, Vol. 20 No. 3, pp. 1144-1156.

Kingery, W.D., Bowen, H.K. and Uhlmann, D.R. (1976), *Introduction to Ceramics*, 2nd ed., John Wiley & Sons, New York, NY, pp. 91-124.

Mock, W., Bartyczak, S., Lee, G., Fredderly, J. and Jordan, K. (2009), "Dynamic properties of polyurea-1000", *Proceedings of the American Physical Society Topical Group on Shock*

Compression of Condensed Matter, Shock Compression of Condensed Matter 2009, American Institute of Physics, Melville, NY, pp. 1241-1244.

Sun, H. (1998), "COMPASS: an ab-initio force-field optimized for condensed-phase applications-overview with details on alkane and benzene compounds", *Journal of Physical Chemistry B*, Vol. 102 No. 38, pp. 7338-7364.

Sun, H., Ren, P. and Fried, J.R. (1998), "The compass force-field: parameterization and validation for phosphazenes", *Computational and Theoretical Polymer Science*, Vol. 8 Nos 1/2, pp. 229-246.

Web references

http://accelrys.com/products/datasheets/materials-visualizer.pdf (accessed November 5, 2013).

http://accelrys.com/products/datasheets/amorphous-cell.pdf (accessed November 5, 2013).

http://accelrys.com/products/datasheets/discover.pdf (accessed November 5, 2013).

About the authors

Mica Grujicic is a Professor of Mechanical Engineering, at the Clemson University. Research interests include computational engineering. Professor Mica Grujicic is the corresponding author and can be contacted at: gmica@clemson.edu

Ramin Yavari is a Graduate Student in Mechanical Engineering at the Clemson University. Research interests include multi-physics modeling of various materials phenomena and processes.

Dr Jennifer Snipes is a Post-doctoral Fellow in Mechanical Engineering at the Clemson University. Research interests include computational material modeling.

Dr S. Ramaswami is a Post-doctoral Fellow in Mechanical Engineering at the Clemson University. Research interests include computational material modeling.

Dr Roshdy Barsoum ia a Manager of Explosion Resistant Coating at the Office of Naval Research. Research interests include shock propagation studies.